



# Effects of the smoothness of partitions of unity on the quality of representation of singular enrichments for GFEM/XFEM stress approximations around brittle cracks

Diego Amadeu F. Torres<sup>a,\*</sup>, Clovis S. de Barcellos<sup>b,1</sup>, Paulo de Tarso R. Mendonça<sup>b,1</sup>

<sup>a</sup> Department of Mechanical Engineering, Federal University of Technology of Paraná - UTFPR, 86036-370 - Londrina, PR, Brazil

<sup>b</sup> Group of Mechanical Analysis and Design, Department of Mechanical Engineering, Federal University of Santa Catarina - UFSC, 88040-900 - Florianópolis, SC, Brazil

Received 1 April 2014; received in revised form 22 August 2014; accepted 28 August 2014

Available online 19 September 2014

## Highlights

- Smoothness around singularities modeled with standard XFEM enrichments is important.
- Comparison between  $C^0$ - and  $C^k$ -GFEM for stress approximation around crack tips.
- Singular and polynomial functions are applied via different patterns of enrichment.
- Effects of smoothness and flat-top property of a mesh-based PoU are analyzed.
- Smoothness improves convergence rates for extrinsically enriched discretizations.

## Abstract

The convergence rates of the conventional generalized/extended finite element method (GFEM/XFEM) in crack modeling are similar to the convergence rates of the finite element method (FEM) (Laborde et al., 2005 and Béchet et al., 2005) unless the crack tip enrichment functions are applied in a subdomain with fixed dimension, independently of the mesh parameter  $h$  and also demanding some special care for blending along the transition zone (Chahine et al., 2006 and Taracón et al., 2009). Thus, to improve convergence rates, more degrees of freedom (DOF) are generated due to the larger quantity of enriched nodes. This work seeks to identify and understand the advantages of better capturing the information provided by singular enrichments over mesh-based smooth partitions of unity (PoU). Such PoU with higher regularity can be built through the so-called  $C^k$ -GFEM framework, following Duarte et al. (2006), based on a moving least square of degree zero and considering mesh-based smooth weighting functions associated with arbitrary polygonal clouds. The purpose herein is to investigate some possible advantages of mesh-based smooth PoU for modeling discontinuities and singularities, in two-dimensional problems of linear elastic fracture mechanics, in such a fashion that the discretization error associated to stress discontinuities inherent in standard  $C^0$ -continuous GFEM/XFEM approximations is eliminated. The procedure shares features similar to the standard FEM regarding domain partition and numerical integration but, as neither the PoU nor the enrichment functions are defined in natural domains, the integrations are performed using only global coordinates. The approximation capabilities of  $C^k$ -GFEM discretizations with different patterns of singular

\* Corresponding author. Tel.: +55 43 3315 6100.

E-mail addresses: [diego.amadeu@gmail.com](mailto:diego.amadeu@gmail.com) (D.A.F. Torres), [clovis.barcellos@ufsc.br](mailto:clovis.barcellos@ufsc.br) (C.S. de Barcellos), [mendonca@grante.ufsc.br](mailto:mendonca@grante.ufsc.br) (P.T.R. Mendonça).

<sup>1</sup> Tel.: +55 48 3721 9899.

enrichment distribution are investigated by analyzing the convergence rates of the  $h$  and  $p$  versions, considering global measures in terms of strain energy and  $\mathcal{L}^2$ -norm of displacements. The effects on stability are also verified by analyzing the evolution of the condition number. The effect of smoothness on conditioning is investigated and the eigenvalues distributions are used to identify the several aspects involved: the smoothness of the PoU, the different types of enrichment functions and the pattern of enrichment. The performance of the smooth approximations is compared to the  $C^0$  counterparts built using conventional  $C^0$  FEM-based PoU. It is shown that smoothness in the presence of extrinsically applied singular enrichments is important, as the information provided by such enrichment is better captured. In addition, there are no stress jumps around singularities, reducing error propagation beyond the neighborhood of the singularity.

© 2014 Elsevier B.V. All rights reserved.

*Keywords:* Arbitrarily smooth GFEM/XFEM; Mesh-based smooth partitions of unity; Crack modeling; Singular stress fields; Enrichment patterns; Convergence analysis

## 1. Introduction

The GFEM and XFEM share the same mathematical fundamentals [1] and were conceived aiming to overcome difficulties related to mesh adaptivity in the conventional FEM. The extrinsic manner of adding algebraic enrichments to an ansatz space is a robust and efficient choice for addressing special information on the features of the solution being sought. The procedure enables adaptive polynomial refinements as different degrees  $p$  of functions can be used according to error oriented algorithms (see [2] [3], for instance). Additionally, any special function can be used, which may avoid changing the characteristic dimension  $h$  of the elements to accommodate localized features such as singularities, boundary layers and material interfaces or represent boundary evolutions without changing the mesh.

In addition to the  $h$  and  $p$  FEM versions commonly used, controlling the regularity  $k$  arises as a refinement option. The use of higher-order continuity functions has not been extensively explored in the community, in contrast to the almost universal use of  $C^0$  functions. Some  $C^1$  approximants that are applied to problems that require such regularity as, e.g., the Hermitian functions in thin plate bending problems (as an alternative to the use of mixed formulation) are either very restrictive or did not become popular, due to the absence of systematic procedures for building such functions to accommodate different element shapes or to allow  $p$ -enrichment by changing the degree of the shape functions. In this scenario, weak forms of  $C^0$  interpolations have been traditionally accepted in finite element analysis, due to the several hindrances that discouraged efforts toward higher regularity approximations.

Nevertheless, certain studies have demonstrated advantages of higher regularity. The term  $k$ -refinement arises for the first time in the work of Reddy and co-workers (see for example [4]), even though the first mesh-based arbitrary smooth approximation was presented by [5]. More recently, [6] also remarked that investigations on the effects of the higher-regularity are of concern.

In this context, the present work investigates the influences exerted by the parameter  $k$  (the regularity of discretizations) specifically in two-dimensional crack modeling through enrichment procedures such as GFEM and XFEM. The motivation for this study rests on the fact that enrichment patterns impart a change on the convergence rates in linear elastic fracture mechanics (LEFM), as extensively discussed by [7,8]. Thus, the smooth GFEM proposed by [9] is exploited in the modeling of singular stress fields using the standard XFEM enrichments of [10]. The quality of the approximations, considering global values as strain energy and the  $\mathcal{L}^2$ -norm of displacements, is investigated. The convergence behavior of discretizations is verified for different patterns of enrichment, simultaneously considering polynomial functions and singular functions. The numerical experiments performed herein were conceived trying to isolate the effects of smoothness, in such a way that other factors which influence convergence, such as special mesh refinements, are avoided.

Throughout this paper,  $C^k$ -GFEM is compared with the standard  $C^0$ -GFEM/XFEM that employs conventional  $C^0$  FEM-based PoU, such as tent functions over simplex elements.

The conditioning of the stiffness matrices is also compared and eigenvalues distributions are obtained in the effort to identify interesting features of smooth GFEM in conjunction with singular enrichments.

The remainder of the paper is organized as follows. Section 2 briefly presents some recent approaches in the field of special mesh-based approximations. This exposition is intended to describe the features, enlighten the similarities, and discuss some possibilities for application of these techniques. Some details regarding smooth GFEM are addressed

in Section 3, where the enrichment functions employed herein are specified and some definitions considered in the investigation are presented. The model problems prepared are discussed in Section 4, and the experiments and corresponding results are discussed in Section 5. Finally, the conclusions are outlined.

## 2. Recent developments on mesh-based approximants

As previously cited, Reddy and co-workers [4] were the first to suggest the  $k$ -refinement through mesh-based functions as a means to improve the quality of approximations, although Edwards [5] proposed an infinitely continuous differentiable ansatz with compact support, based on convex clouds defined by patches of elements.

Higher-order regularity shape functions with hierarchical  $p$  character are proposed in [4] to recover the smoothness of the approximated FE solutions. The functions proposed by the authors are defined in intrinsic coordinates, and their inter-element continuity, even after mapping, follows from the fact that both the functions values and their higher order derivatives are nodal degrees of freedom. The functions for higher spatial dimensions are built from the tensor product of one-dimensional functions. On the other hand, the construction of mesh-based smooth functions reported by Edwards [5] employs the Shepard equation [11] to define a partition of unity based on continuously differentiable weighting functions, allowing to keep the conventional structure of irreducible displacement-based formulations. Such smooth weighting functions are built by a product of cloud edge functions which, in turn, are functions defined in global (physical) coordinates that smoothly decreases to zero toward the edges of the cloud and are strictly positive inside the it.

Edwards' original procedure, based on a simple product, fails in the case of a non-convex cloud. To solve this restriction [9] proposed the use of Boolean  $R$ -functions to enable the building of smooth PoU for non-convex polytopes with arbitrary  $k$  regularity.  $R$ -functions [12,13] are logically charged real functions whose signs are completely determined by the signs of their arguments, and are independent of the magnitude of the arguments.

The Shepard PoU is simply the moving least square (MLS) [14] approximation of polynomial degree zero, i.e., using only a constant function in the basis, and is also used in other mesh-free methods such as the finite spheres [15] and the particle-partition of unity [16] methods. Generally, the approximation in mesh-free methods is built using the MLS method as, for instance, the Element Free Galerkin (EFG) method [17]. This procedure promotes  $p$  enrichment intrinsically, that is, higher-order polynomial terms are added without creating new unknowns associated with the nodes. Special functions, such as discontinuous ones, may also be introduced in the MLS approximation [18], but special care is needed to guarantee conformity, as MLS did not originally allow the enrichments to vary along the domain [19]. This detail distinguishes the EFG method from  $hp$ -clouds method [20–22], which only employs the MLS through the Shepard equation to define a PoU over which enrichments are applied extrinsically (similarly to PUFEM, see [23]).

Extrinsic enrichment is characterized by adding unknowns to the nodes, such that each additional unknown is associated with a new applied enrichment functions (see, for instance, [24–28]). Therefore, the PoU functions can be called “pasting functions” as they bring about implicit domain discretization (defining compact supports), merge various local approximations by performing an unbiased average, and determine their order or continuity across element boundaries [29].

Another approach that proposes to enhance the regularity of a mesh-based approximation and that has gained attention recently is the smoothed FEM [30]. This methodology proposes to employ a smoothing operation [31], such as a non-local gradient operation, which was originally designed to improve the nodal integration method [32] which, in turn, was proposed to eliminate the background mesh in the EFG method.

In the smoothed FEM, the strain field is projected onto a set of constant fields based on smoothing cells generated by a partitioning within each element. Thus, the smoothing operation is performed for each smoothing cell, and by choosing a constant smoothing function the area integration over the cell becomes a line integration along its boundaries [30]. In this way, because only the FE shape functions are used in the line integration, the averaged and non-mapped Lagrange functions are generally applied. Therefore, no coordinate mapping is required as the only function manipulated is the displacement function along the edges of the smoothing cells.

Unfortunately, the original smoothed FEM renders an approximation that cannot be explicitly known at certain points of the smoothed FE, in the case of certain distorted geometries. This unknowability is as a consequence of the non-mapped Lagrangian shape functions [33]. For this reason, [34] proposed to use the Wachspress interpolation [35,36] as an alternative to suppress the problems related to the existence, non-negativity and linearity of non-mapped Lagrangian shape functions.

A Wachspress interpolation employs rational (ratio of polynomial functions) generalized barycentric coordinate-based functions built on arbitrary polygonal elements. It is surprising that the basic idea behind the Wachspress rational functions is the Shepard equation, considering weighting functions defined as a product of distance functions, in the case of convex  $n$ -gons [37]. As in the  $C^k$ -GFEM procedure, the Wachspress interpolant can define an approximation over arbitrary polytopes requiring some special care in the case of non-convex elements [37] to avoid null values of the weighting function inside the element.

The distance functions used as element edge functions are responsible for imputing linear reproducibility to the Wachspress interpolation. Thus, the Wachspress interpolation is the simplest function construction that satisfies both linear reproducibility and independence (in the sense of linear independence), defines a PoU and also shows the Kronecker delta property for arbitrary  $n$ -gons [37]. It is important to note that the only difference between the Wachspress interpolant and its Edwards counterpart is the nature of the edge functions. In the former method, the resultant PoU exhibits  $C^0$  regularity while the exponential edge functions in the Edwards method lead to  $C^\infty$  PoU. It is also clear that Wachspress-based smoothed FEM and the  $C^k$ -GFEM are completely free of geometrical restrictions and, as both are directly computed in physical coordinates, they can be highly appropriate for distorted meshes (see [34,27]).

Additionally, for a regular  $n$ -gon (all angles are equal in measure) the Wachspress shape functions are identical to the Laplace shape functions [38]. The latter is a natural neighbor interpolant and is the simplest and most popular Voronoi-based interpolation method on polygonal elements [39]. Laplace shape functions have also been used in topological optimization problems, as in [40], in which shape functions for polygonal elements were used to avoid mesh dependences that stem from the basic geometric features of conventional discretizations. Laplace interpolants were also used for crack modeling in [41], over which were applied the conventional enrichment functions of XFEM.

It is possible to note that higher-degree reproducibility and higher-order continuity of mesh-based PoU functions are features that generally are not obtained simultaneously. Recovering a degree of reproducibility for mesh-based functions with some order of smoothness could be attempted by considering maximum-entropy (Max-Ent) methodology. The shape functions in the Max-Ent framework can be seen as probability distributions with a specific approximation constraint, such as a certain degree of reproducibility. For instance, if only zero-degree consistency is required, the Max-Ent functions are Shepard approximants with Gaussian weighting functions [42]. However, the higher smoothness of Max-Ent functions is dependent to a lower degree of locality, in such a way that their supports are enlarged and they overlapping extensively. Thus, these functions also lose the Kronecker delta property and make numerical integration more difficult. Enlarging supports also impacts the sparsity, which is a feature that  $C^k$ -GFEM does not show. Recently, crack tip enrichment functions were applied as an extrinsic enrichment over Max-Ent discretizations [43] to verify certain advantages of smoothness in the approximation of high gradients. Smoothness can lead to better rates of convergence but it is necessary to set an appropriate locality parameter of the Max-Ent functions to balance the cost of numerical integration and accuracy.

Therefore, from the exposition so far, it can be seen that some features, such as being mapping-free, the absence of geometric restrictions, and some order of smoothness are attractive features. Another quality that has been noted as desirable for a PoU is the flat-top property, specially in the context of enrichment procedures [44,45], in which the linear dependence of the functions in the ansatz is of concern. In GFEM/XFEM, if the both enrichment functions and PoU are polynomial, the stiffness matrix becomes singular [24,46]. In contrast, for PoU functions with the flat-top property, if the set of enrichment functions is linearly independent, then the enriched subspace will also be linearly independent over the PoU's flat-top.

Notably, the conventional FE shape functions used in XFEM/GFEM are mesh-based closed-form functions with simple numerical integration but (a) they require coordinate mapping, (b) they render lower regularity and (c) they lead to ill-conditioned or singular stiffness matrices (when the PoU is enriched with the usual simple set of polynomials, as that used in [24,26], for instance). Differently, meshfree PoU functions only demand nodes or particles with supports defined by the corresponding radius and produce higher regularity, but they do not exhibit a simple and predictable overlapping pattern and are generally associated with complicated numerical integrations. Furthermore, imposing an essential boundary condition is difficult in both PoU constructions. For example, a strong-form essential boundary condition enforcement is not trivial for general boundaries and even homogeneous conditions demand some care in conventional GFEM approximations [26,27].

Although in meshfree methods it is possible to conveniently select cloud radii to obtain non-empty flat-tops, such a feature is not common for a PoU. For this reason, some attempts have been addressed aiming to conceive an effective

procedure for building mesh-based PoU with flat-top property. Toward this goal, [47] proposed an one-dimensional piecewise polynomial PoU construction in which the flat-top dimension is defined a priori but without a closed-form, and from which the higher dimension versions are obtained by a tensorial product. Thus, the procedure uses a simple subdivision of the domain into disjoint polygons. Consequently, the overlapping can be simply detected, and the numerical integration scheme is favored. However, such a method impose geometric restrictions on the domain partition and on curved boundaries.

A more recent approach that produces a PoU with an a priori defined flat-top dimension is the work of [48]. This methodology considers quadrilateral finite element meshes, and the topology of the flat-top portions is a consequence of the mesh because the transitions, between PoU functions, are defined by narrow bands along the edges, whose width is previously chosen. Thus, to obtain a closed-form description, Lagrangian shape functions are used to compose the transition. Therefore, the resultant PoU has fewer geometric restrictions than the procedure of [47], enables easier integration and easier enforcement of essential boundary conditions, and can be used for extrinsic enrichment. Nevertheless, it is minimally conforming again, with  $C^0$  regularity.

Consequently, it can be argued that the flat-top property is another desirable feature of a PoU for enrichment-based methods in addition to higher-order regularity, the absence of geometric restriction and coordinate mapping. In this scenario, the  $C^k$ -GFEM PoU satisfies all these requirements and it is possible to conclude that it combines the advantages associated with extrinsic enrichment. This especial instance of the generalized/extended FEM allows to recover the smoothness commonly generated by meshfree approximations using element meshes for cloud definition.

The construction of nodal weighting functions through a combination of cloud edge functions is completely free of geometrical restrictions [9]. Any type of conventional domain partitioning can be used, in such a way that the choice of the element shape is oriented aiming to employ it directly as an integration cell. For instance, quadrangular elements were used in [9] and triangular elements were used in [27,28].

Moreover, it is remarkable that in the  $C^k$ -GFEM the regularity can be increased only setting conveniently chosen smooth cloud edge functions, without enlarging the support of the PoU functions, thus avoiding extensive overlapping and more populated stiffness matrices. Additionally, the resulting PoU functions have the Kronecker delta property, unlike the other smooth approximations options. Finally, the Shepard equation enables the combination of weighting functions with different smoothness. In [49] it is shown that coupling  $C^k$  and  $C^0$  mesh-based weighting functions would be possible, allowing the application of higher regularity only where it is convenient.

### 3. Smooth GFEM-based approximations

The purpose of such a smooth version of GFEM is to build approximations with arbitrary continuity, maintaining all interesting features of a PoU-based method. Thus, continuous stress fields may be obtained for mesh-based approximations without enlarging the overlapping of basis functions, while maintaining the key characteristic of FEM implementations regarding domain partitioning, numerical integration and boundary conditions enforcement.

Mesh-based arbitrary continuous approximation functions can be built through the so-called  $C^k$ -GFEM framework, following Duarte and collaborators [9]. This approach employs a MLS approximation of polynomial degree zero (Shepard equation) considering smooth weighting functions as in the *hp*-cloud method [20] for defining a PoU. The last considers circular (or spherical) clouds, similarly to other meshfree methods, whereas the former treats arbitrary polygonal patches of elements as clouds. Cloud edge functions with the desired continuity are combined to generate the weighting functions, which are used to define the PoU. Therefore, the resulting PoU can be described as a special instance of the *hp*-cloud method.

In this way, to define the discretized version of the variational boundary value problem under analysis (Section 4), a conventional finite element triangulation,  $\{\mathcal{K}_e\}_{e=1}^{NE}$  ( $NE$  being the number of elements in  $\mathcal{K}_e$ ), defined by  $N$  nodes with coordinates  $\{\mathbf{x}_\alpha\}_{\alpha=1}^N$ , for an open-bounded polyhedral domain  $\Omega \subset \mathbb{R}^2$ , is considered. Defining the interior of the union of the finite elements sharing each node  $\mathbf{x}_\alpha$  as a *cloud*  $\omega_\alpha$ ,  $\alpha = 1, \dots, N$ , an open covering  $\mathfrak{S}_N$  of the domain  $\Omega$  is built by the collection of  $N$  clouds, that is, the closure  $\bar{\Omega}$  of the domain is contained in the union of the cloud closures  $\bar{\omega}_\alpha$ , such that  $\bar{\Omega} \subset \bigcup_{\alpha=1}^N \bar{\omega}_\alpha$ .

In addition, if a set of functions  $\mathfrak{S}_N = \{\varphi_\alpha(\mathbf{x})\}_{\alpha=1}^N$ , each one having the corresponding cloud  $\omega_\alpha$  as its compact support, has the property that  $\varphi_\alpha(\mathbf{x}) \in C_0^k(\omega_\alpha)$ ,  $k \geq 0$  and  $\sum_{\alpha=1}^N \varphi_\alpha(\mathbf{x}) = 1$ ,  $\forall \mathbf{x} \in \Omega$ , and every compact subset of  $\Omega$

intersects only a finite number of clouds, then such a set  $\mathfrak{S}_N$  is termed a Partition of Unity (PoU) subordinated to the covering  $\mathfrak{S}_N$  [50]. There are several types of PoU used in computational mechanics and the conventional FEM shape functions, such as tent functions for simplex triangles or bilinear Lagrangian functions for quadrangular elements, are simply certain types that only have  $C_0^0(\omega_\alpha)$  continuity. The Shepard scheme is another example that uses *weighting functions*,  $\mathcal{W}_\alpha : \mathbb{R}^2 \rightarrow \mathbb{R}$ , with the cloud  $\omega_\alpha$  as their compact support. The Shepard PoU functions subordinated to the covering  $\mathfrak{S}_N$  are defined as

$$\varphi_\alpha(\mathbf{x}) = \frac{\mathcal{W}_\alpha(\mathbf{x})}{\sum_{\beta(\mathbf{x})} \mathcal{W}_\beta(\mathbf{x})}, \quad \beta(\mathbf{x}) \in \{\gamma \mid \mathcal{W}_\gamma(\mathbf{x}) \neq 0\}. \quad (1)$$

Therefore, the regularity of the Shepard PoU functions relies only on the regularity of the weighting functions  $\mathcal{W}_\alpha$ . To reduce the computational time and to simplify the implementation, the  $C^k$ -GFEM scheme employs element meshes to define the clouds. It is important to note that there is no limitation for the overlapping of clouds and no restriction on the shape of clouds and its elements. For example, the weighting function  $\mathcal{W}_\alpha$  for a convex cloud  $\omega_\alpha$  can be simply defined as the product of all cloud edge functions  $\varepsilon_{\alpha,j}(\xi_j)$  as

$$\mathcal{W}_\alpha(\mathbf{x}) := \prod_{j=1}^{M_\alpha} \varepsilon_{\alpha,j}(\xi_j(\mathbf{x})) \quad (2)$$

where  $M_\alpha$  is the number of *cloud edge functions*  $\varepsilon_{\alpha,j}$  associated with the cloud  $\omega_\alpha$ , defined in terms of the parametric coordinates  $\xi_j$  normal to each edge  $j$  [51,9].

According to Edwards [5], a cloud edge function is a strictly positive function inside the cloud that vanishes, together with all its derivatives, toward an edge, rendering a  $C_0^\infty(\omega_\alpha)$  weighting function. Edwards proposed to use the following definition for this infinitely smooth cloud edge function  $\varepsilon_{\alpha,j}$ , for the edge  $j$  of a cloud  $\omega_\alpha$

$$\varepsilon_{\alpha,j}(\mathbf{x}) := \begin{cases} e^{\frac{1}{(1/(\xi_j(\mathbf{x}))^\gamma)}} = e^{-\xi_j^{-\gamma}} & , \text{ if } \xi_j > 0, \\ 0 & , \text{ otherwise} \end{cases} \quad (3)$$

where  $\gamma$  is a positive constant. The parametrization is considered only to scale the several edge functions of a cloud in order to have all of them unitary at the cloud node, and with the same decaying rate  $\beta$  (see [9,51]), to reduce mesh dependences. However, many functions beyond exponential ones meet the requirements of having  $k$  derivatives that are null on the edge. For example, in [51] polynomial edge functions were subjected to numerical investigations. But in case of polynomial cloud edge functions the continuity is limited independently of the cloud geometry.

At this point, it is possible to note the similarity between  $C^k$ -GFEM and Wachspress interpolations [37], as the latter considers an arbitrary polygonal element instead of a cloud to build a shape function, using the Shepard equation with weighting functions defined from linear edge functions.

Herein, exponential edge functions are used, exactly following the procedure described in [51], using  $\gamma = 0.3$  and  $\beta = 0.6$ , which leads to  $C^\infty(\Omega)$  approximations for meshes with only convex clouds, because the definition of the weighting functions (2). In contrast, in the case of non-convex clouds, it is necessary to replace the edge functions of a pair of non-convex edges with a single new edge function obtained through a Boolean product [52] before performing the weighting functions computation, as proposed by [9].

As previously cited, the procedure shares similarities with the standard FEM regarding the domain partition and integration procedures. Although the process for constructing continuous PoU is quite versatile, allowing for free-form clouds, the need for the so-called background grid for domain integration (as in meshfree methods) suggests that the cloud definition using triangular or quadrilateral meshes is highly appropriate, as there are simple quadrature rules to be used. Additionally, as neither the PoU nor the enrichment functions are defined in natural domains, the integrations are performed using only global coordinates, which makes the  $C^k$ -GFEM very robust to mesh distortions [27]. Clearly, the PoU set  $\mathfrak{S}_N = \{\varphi_\alpha(\mathbf{x})\}_{\alpha=1}^N$  defined by (1) can only represent a rigid body motion, which means zero-degree reproducibility. Consequently, enrichments must be extrinsically added to enhance the approximation properties of the ansatz spaces. In this study, polynomial functions such the ones used in [26] are applied simultaneously to special functions, as proposed by [10], in order to represent certain features of the solution (see Fig. 1).

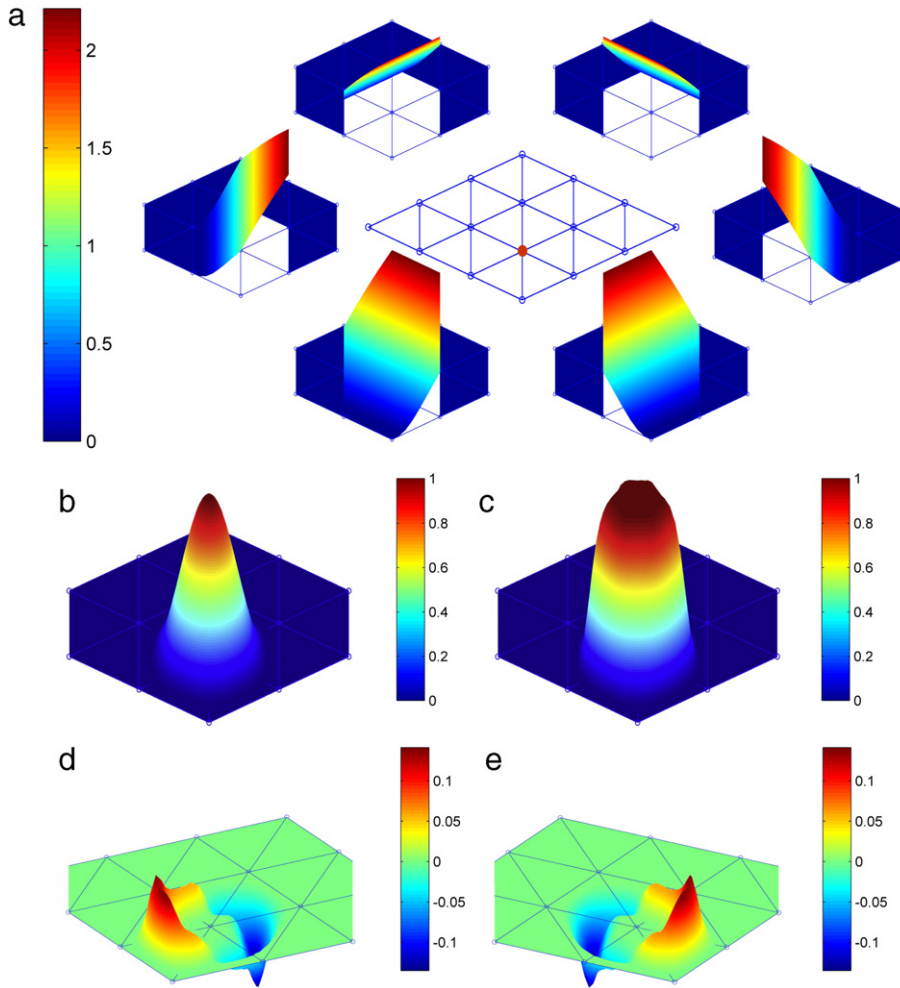


Fig. 1. Construction of a smooth PoU following the  $C^k$ -GFEM framework: (a) the set of exponential cloud edge functions for the red node, built following the definition (3), whose cloud is composed of six triangular elements and for which the characteristic dimensions are  $h_x = h_y = 30.0$ . As the cloud is convex, a weight function (b) is built through a simple productory (2) of the edge functions in (a). The MLS of degree zero, the Shepard (1), provides a smooth PoU (c), which has a flat-top as seen by the nullity of derivatives along axis  $x$  (d) and  $y$  (e) in the vicinity of the node.

Then, according to the extrinsic enrichment procedure, an approximation for the cartesian  $x$ -component of displacement,  $\tilde{u}_x(\mathbf{x})$ , for instance, is defined as

$$\tilde{u}_x(\mathbf{x}) = \sum_{\alpha=1}^N \varphi_{\alpha}(\mathbf{x}) \left\{ u_{\alpha} + \sum_{i=1}^{q_{\alpha}^p} \mathcal{L}_{\alpha i}^p(\mathbf{x}) b_{\alpha i}^p + \sum_{l=1}^{q_{\alpha}^s} \mathcal{L}_{\alpha l}^s b_{\alpha l}^s(\mathbf{x}) \right\} \quad (4)$$

where  $u_{\alpha}$ ,  $b_{\alpha i}^p$  and  $b_{\alpha l}^s$  are the nodal parameters associated with the PoU function  $\varphi_{\alpha}(\mathbf{x})$ , and with the polynomial ( $p$ ) and singular ( $s$ ) enriched functions,  $\varphi_{\alpha}(\mathbf{x})\mathcal{L}_{\alpha i}^p(\mathbf{x})$  and  $\varphi_{\alpha}(\mathbf{x})\mathcal{L}_{\alpha l}^s(\mathbf{x})$ , respectively.

In (4),  $q_{\alpha}^p$  is the number of polynomial enrichment functions of the node  $\mathbf{x}_{\alpha}$  such that in the case of  $p = 2$ , for instance, the set of enrichments is given by

$$\mathcal{L}_{\alpha i}^2(x, y) = \left\{ \bar{x}, \bar{y}, \bar{x}^2, \bar{x}\bar{y}, \bar{y}^2 \right\}, \quad i = 1, 2, \dots, 5 \quad (5)$$

where a translation and a scaling are performed (similar to [26]) to reduce the mesh dependences. The first enrichment function of (5), for example, is given by the normalized coordinate  $\bar{x}$  such that  $\bar{x} := (x - x_{\alpha})/h_{\alpha x}$ , with the

$x$ -coordinate  $x_\alpha$  of the node used for translation and the characteristic length  $h_{\alpha_x}$  of the cloud, taken as the  $x$ -projection of the largest distance from the node  $\mathbf{x}_\alpha$  to each of their cloud edges, used for scaling. A similar definition is used for  $\bar{y}$ .

Additionally,  $q_\alpha^s$  is the number of *branch functions* of each node, such that  $q_\alpha^s = 0$  or 4, depending on whether or not the node is enriched with crack tip functions. This last set of functions, namely

$$\mathcal{L}_{\alpha 4}^s(r, \theta) = \left\{ \sqrt{r} \sin\left(\frac{\theta}{2}\right), \sqrt{r} \cos\left(\frac{\theta}{2}\right), \sqrt{r} \sin\left(\frac{\theta}{2}\right) \sin(\theta), \sqrt{r} \cos\left(\frac{\theta}{2}\right) \sin(\theta) \right\} \quad (6)$$

is responsible for generating the discontinuity of a straight crack segment and the singularity in the vicinity of its tip, as proposed by [10,53], with  $r$  and  $\theta$  related to a local polar coordinate system placed at the crack tip.

**Remark 1.** It should be noted that the usual structure of the standard displacement-based FEM is preserved in this smooth version of GFEM. The entire  $C^k$ -GFEM formulation, summarized in this section, enters the program structure encapsulated in a single routine, that computes the set of approximation functions values and its derivatives in the same fashion as for FEM functions, which are subsequently used to compute the element contributions.

Therefore, the discretized variational problem for the linear elastostatic problem is: *find an approximation  $\tilde{\mathbf{u}} \in \mathcal{U}_h(\Omega)$ , for the displacement field  $\mathbf{u} = \{u_x, u_y\}^T \in \mathcal{U}$ , such that  $\mathcal{B}(\tilde{\mathbf{u}}, \tilde{\mathbf{v}}) = \mathcal{L}(\tilde{\mathbf{v}})$ ,  $\forall \tilde{\mathbf{v}} = \{\tilde{v}_x, \tilde{v}_y\}^T \in \mathcal{V}_h$* , where the approximation  $\tilde{\mathbf{u}}$  is an entity of a subspace  $\mathcal{U}_h \in \mathcal{U}$  spanned by a set of kinematically admissible GFEM approximation functions. The subspace  $\mathcal{V}_h$  of admissible variations is conventionally defined [54]. The bilinear form  $\mathcal{B}(\bullet, \bullet)$  and the linear functional  $\mathcal{L}(\bullet)$ , that correspond to the elliptic partial differential equilibrium equation  $\mathbf{L}^T \boldsymbol{\sigma}(\mathbf{u}) + \mathbf{b} = \mathbf{0}$  in  $\Omega$ , are defined as

$$\mathcal{B}(\tilde{\mathbf{u}}, \tilde{\mathbf{v}}) := \int_{\Omega} \boldsymbol{\varepsilon}^T(\tilde{\mathbf{v}}) \boldsymbol{\sigma}(\tilde{\mathbf{u}}) l_z d\Omega \quad \text{and} \quad \mathcal{L}(\tilde{\mathbf{v}}) := \int_{\Omega} \tilde{\mathbf{v}}^T \mathbf{b} l_z d\Omega + \int_{\Gamma_N} \tilde{\mathbf{v}}^T \bar{\mathbf{t}}_z ds \quad (7)$$

where  $l_z$  is the thickness of the body, assumed here to be a constant. The body is loaded by the applied volume forces  $\mathbf{b} = \{b_x, b_y\}^T$  (the superscript  $T$  indicates transpose) and surface traction  $\mathbf{t} = \{t_x, t_y\}^T$ ,  $\mathbf{t} = \boldsymbol{\sigma}(\mathbf{u})\mathbf{n} = \bar{\mathbf{t}}$  on  $\Gamma_N$ . The stresses,  $\boldsymbol{\sigma} = \{\sigma_x, \sigma_y, \tau_{xy}\}^T$ , are related to the strains,  $\boldsymbol{\varepsilon} = \{\varepsilon_x, \varepsilon_y, \gamma_{xy}\}^T$ , through the linear elastic relation  $\boldsymbol{\sigma}(\mathbf{u}) = \mathbb{C} \boldsymbol{\varepsilon}(\mathbf{u})$ , where  $\mathbb{C}$  is a constitutive matrix. The strains are related to the displacements by  $\boldsymbol{\varepsilon}(\mathbf{u}) = \mathbf{L}\mathbf{u}$ . Finally, the differential operator  $\mathbf{L}$  and the normal vector  $\mathbf{n}$  are defined as

$$\mathbf{L} = \begin{bmatrix} \frac{\partial}{\partial x} & 0 \\ 0 & \frac{\partial}{\partial y} \\ \frac{\partial}{\partial y} & \frac{\partial}{\partial x} \end{bmatrix} \quad \text{and} \quad \mathbf{n} = \begin{bmatrix} n_x & 0 & n_y \\ 0 & n_y & n_x \end{bmatrix}. \quad (8)$$

**Remark 2.** The equilibrium is stated herein using a weak formulation, as commonly employed in FEM. However, as pointed by [4], higher-order continuous approximation functions may encourage the elimination of weak forms and the use of weighted residual methods based directly on the original differential equilibrium equations. This type of strategy is viable if it is not imperative to obtain symmetric matrices [55]. In this sense, the availability of systematically built higher-order regularity approximations have motivated to reconsider, e.g., collocation methods [56] for structural analysis and hence, the  $C^k$ -GFEM is also applicable.

**Remark 3.** When the PoU is built from polynomial FE shape functions, as in conventional GFEM, the linear algebraic system resulting from the variational equilibrium equation under study using (4) is linearly dependent [24]. In the present case, where the PoU is built as quotients of exponential functions, the resulting global stiffness matrix is positive definite if the boundary conditions imposed are sufficient to prevent rigid body motions.

**Remark 4.** While the conventional PoU of the standard GFEM/XFEM (such as tent functions for triangular meshes) can generate a complete polynomial of degree one, over the domain, the present  $C^k$  PoU is only capable of reproducing

a constant function, as an instance of the Shepard approximation [57]. Thus, following the notation established in [27,28], when the  $C^k$  PoU is extrinsically enriched with a polynomial set of degree  $p$  (similar to (5)) to improve the reproducibility, the approximation functions form a basis for polynomials of degree  $b = p$ . In contrast, for  $C^0$  PoU functions over simplex elements, the enriched basis can reproduce polynomials of degree  $b = p + 1$  when the polynomial enrichment involves a set of enrichment functions of degree  $p$ , as the  $C^0$  PoU already has first-degree consistency.

#### 4. Model problem

The classical problem of a pure Mode-I opening crack for LEFM with prescribed stress intensity factors  $K_I = 1.0$  and  $K_{II} = 0.0$  is analyzed, considering the plane strain state and traction boundary conditions applied according to the analytical solution [58]. Such a problem was chosen to have exact values for assessing the quality of the approximations.

For this purpose, a quadrilateral domain  $\bar{\Omega} = [0, 2a] \times [0, 2a]$ , whose characteristic dimension is  $a = 60.0$  and with constant thickness  $l_z = 1.0$ , is considered. A straight crack defines a segment boundary  $\Gamma_C = [0, a] \times \{a\}$ . The linear elastic material has Young modules  $E = 1.0$  and Poisson ratio  $\nu = 0.3$ .

The goal here is to verify the ability of smooth GFEM functions to approximate stress fields around the crack tip. For comparison, the same problem is modeled using standard  $C^0$ -GFEM functions, whose PoU functions are the conventional tent functions for simplex triangles.

The enrichment functions commonly used to represent the discontinuity along a crack path and the singularity at the crack tip, the *Heaviside* and *branch functions*, respectively, were originally applied only to the nodes along a narrow band along the crack [10,53,59]. This strategy, termed a **topologic** enrichment pattern by [8,7], was employed in the earliest investigations.

But, unlike of the standard XFEM/GFEM procedure, as only a straight crack is considered in this model problem, the nodes along the crack path were also enriched with branch functions instead of *Heaviside* functions. The option to use only branch functions (6) to represent the entire crack<sup>3</sup> is chosen to minimize transition effects, despite consuming more DOF. Additionally, the polynomial  $p$  refinement, similar to (5), is applied to flexibilize the transition zone between the portion enriched with singular functions and the remainder of domain and to capture the Neumann boundary conditions, in the case of uniform  $p$  enrichment. More details on the patterns of enrichment will be given in the following section.

#### 5. Numerical results

In this work, the quality of the approximations is verified through global measures such as the strain energy or  $\mathcal{L}^2(\Omega)$ -norm of displacements. The values computed for the approximated solutions are compared to the exact ones, and the relative errors are plotted against the number of DOF consumed by the discretizations.

The strain energy is defined as

$$U(\mathbf{u}) = \frac{1}{2} \int_{\Omega} \int_{\Omega} \boldsymbol{\sigma}^T \boldsymbol{\varepsilon} l_z dx dy \quad (9)$$

considering the notation presented in Section 3. The exact value of the strain energy for the model problem was computed by the authors and is given by

$$U(\mathbf{u}_{EX}) = 2.979\ 042\ 724\ 126\ 056(A_1)^2 a l_z/E \quad (10)$$

where  $A_1 = K_I/\sqrt{2\pi}$ , for a prescribed stress intensity factor  $K_I$ . The first seven digits of the constant in (10) agrees with the value given by [60] in which only seven digits were provided.

<sup>3</sup> The crack representation was performed using only branch functions in order to reduce sources of blending/transition effects. The authors are also concerned with transition effects which manifest through anomalous reductions in the rates of convergence due to partially enriched elements. Thus, the clear identification of the behavior of higher-regularity along the transition zone, near the crack tip, considering only branch functions, becomes easier when compared to a situation where two types of enrichments are simultaneously applied.

On the other hand, the  $\mathcal{L}^2(\Omega)$ -norm of displacements is also used, defined as

$$\|\mathbf{u}\|_{\mathcal{L}^2(\Omega)} = \left( \int \int_{\Omega} (\mathbf{u}^T \mathbf{u}) \, dx \, dy \right)^{\frac{1}{2}} \quad (11)$$

also using matrix notation, whose exact value as computed by the authors is

$$\|\mathbf{u}_{EX}\|_{\mathcal{L}^2(\Omega)} = \left( 19.345 \, 984 \, 181 \, 934 \, 81 (A_1)^2 a^3 l_z / E^2 \right)^{1/2}. \quad (12)$$

The relative error is defined as usual and in the case of the strain energy, for instance, is computed as

$$er(U) = \frac{U(\mathbf{u}_{EX}) - U(\mathbf{u}_p)}{U(\mathbf{u}_{EX})} \quad (13)$$

and a similar computation is used for the other quantity.

In the sequence, a series of experiments is conducted to identify certain advantages of using smooth PoU functions for crack modeling. The manner in which the singular enrichment is applied around the crack tip and some treatment on the transition zone (blending elements [61,62]) impart the discretization performance.

It is known that one option for enhancing the convergence rates in conventional  $C^0$ -GFEM/XFEM is to apply the singular enrichment on a set of nodes contained inside a zone of fixed dimension, independently of the mesh parameter  $h$ , which is called the **geometric** enrichment pattern. Such geometric enrichment was conceived because, for mesh refinements in conventional  $C^0$ -GFEM/XFEM enriched via the topologic pattern, it is noted that the convergence rates are not improved if compared to the standard FEM [63,8,7].

Thus, following this conclusion, the geometric pattern of enrichment with singular functions is the first strategy studied herein.

### 5.1. Geometric pattern of enrichment

Initially, it should be mentioned that appropriate mesh refinement strategies, such as those proposed by [64,65] for problems with singularities (radical or geometrical meshes), were not applied herein aiming to isolate the effects of the smoothness of the PoU and polynomial enrichments.

The first situation studied considers crack opening over element edges, for which four uniform meshes with different  $h$  parameters shown in Fig. 2 are used, namely M1 to M4. The crack representation is obtained through enrichment, with branch functions (6), of the nodes inside two circular regions of radius  $R1 = 42.50$  and  $R2 = 30.00$ , illustrated in blue and red, respectively. Additionally, the branch functions are also applied on the orange nodes to make a complete representation of the crack path (some additional orange nodes are necessary in the case of the R2 circle). On the other hand, polynomial enrichment functions (5) are uniformly applied along the domain.

This case is proposed because it is more convenient for  $C^0$  approximations to have the discontinuity over element edges and the singularity over a node. For the meshes of Fig. 2 the rigid body motions are suppressed by applying the restrictions  $u_x(a, a) = u_y(a, a) = u_y(2a, a) = 0$ . These restrictions are chosen because, for the Mode I boundary traction distribution, reaction forces do not occur at these positions.

It is also necessary to assess the performance of  $C^k$  approximations for situations in which the crack crosses elements, as the extrinsically enriched procedures enable the modeling of cracks independently of the mesh topology (in fact, this ability is the reason these methods have been developed). Thus, the problem of Mode I crack opening was also analyzed considering the four meshes shown in Fig. 3 where the crack path and its tip are not coincident with element edges and a node, respectively. The details about the applied enrichments are the same as early discussed for the case with crack along element edges. The geometry and material properties are the same as in the first study. For these meshes, the applied essential boundary conditions are  $u_x(2a, 0) = u_y(2a, 0) = u_x(2a, 2a) = 0$ .

Herein, only meshes with all clouds convex are employed and, therefore, the  $C^k$ -GFEM approximations reported are infinitely smooth, that is, with  $k = \infty$ . It should be noted that this higher-order smoothness is obtained without enlarging the supports of the functions and, consequently, the sparsity for  $C^k$ -GFEM is the same as for  $C^0$ -GFEM/XFEM, which implies the same computational effort to factorize the stiffness matrix.

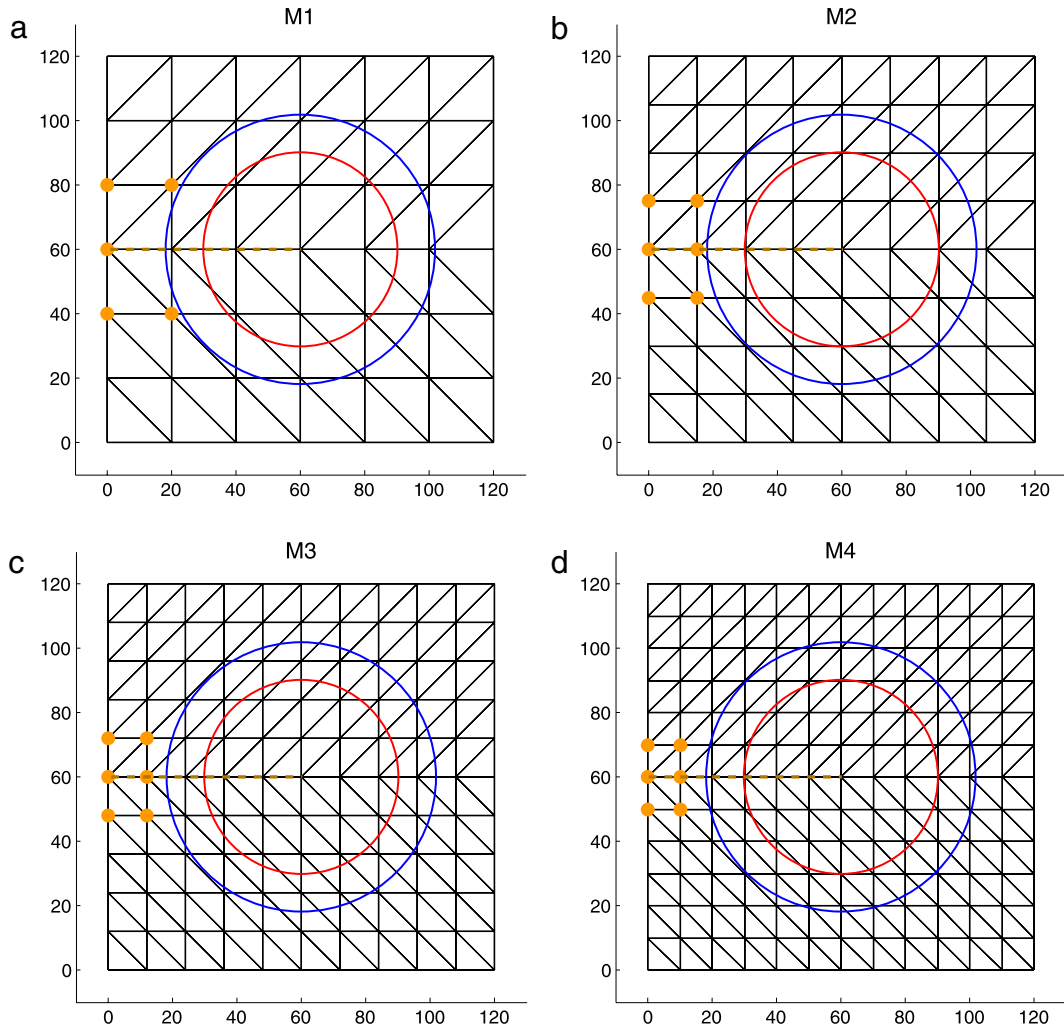


Fig. 2. Discretizations for which the crack opens over element edges, such that  $\Gamma_C = [0, 60] \times \{60\}$ , noting that the crack tip falls on a node (the crack is along the dashed brown line). Singular enrichment functions (6) are applied according to the geometric pattern. Polynomial enrichment functions (5) are uniformly applied along the domain. (For interpretation of the references to color in this figure, the reader is referred to the web version of this article.)

### 5.1.1. Accuracy of numerical domain integration

The issue of numerical integration of singular enrichment functions for GFEM/XFEM has been regularly addressed (see [66–69], for instance). In this work, an additional difficulty arises due to the rational nature of  $C^k$ -GFEM PoU functions. In the case of regular problems, using only polynomial enrichment functions, the cost for numerical integration of  $C^k$ -GFEM approximations has been extensively investigated in [51,27,28].

As a first approach regarding singular enriched smooth GFEM discretizations, a special effort was made to reduce numerical integration errors to negligible levels.

In the case of elements cut by the crack, a subdivision in cells was performed, as usual. To integrate elements or cells containing the singularity, a special scheme was devised. This integration scheme employs a sequence of procedures: (a) first,  $15 \times 15$  Gauss–Legendre points are mapped by a Lachat–Watson transformation [70], similar to the quasi-polar mapping used in [66] or [8], and (b) subsequently they are moved according to a quarter-point mapping, inspired by [71]. Then, at the neighborhood of the singularity, the quarter-point mapping is responsible for moving the integration points toward the crack tip. For the remaining elements or integration cells, the Wandzura’s triangular rule [72] with 175 points was applied. Fig. 4 displays some situations and their respective integration points.

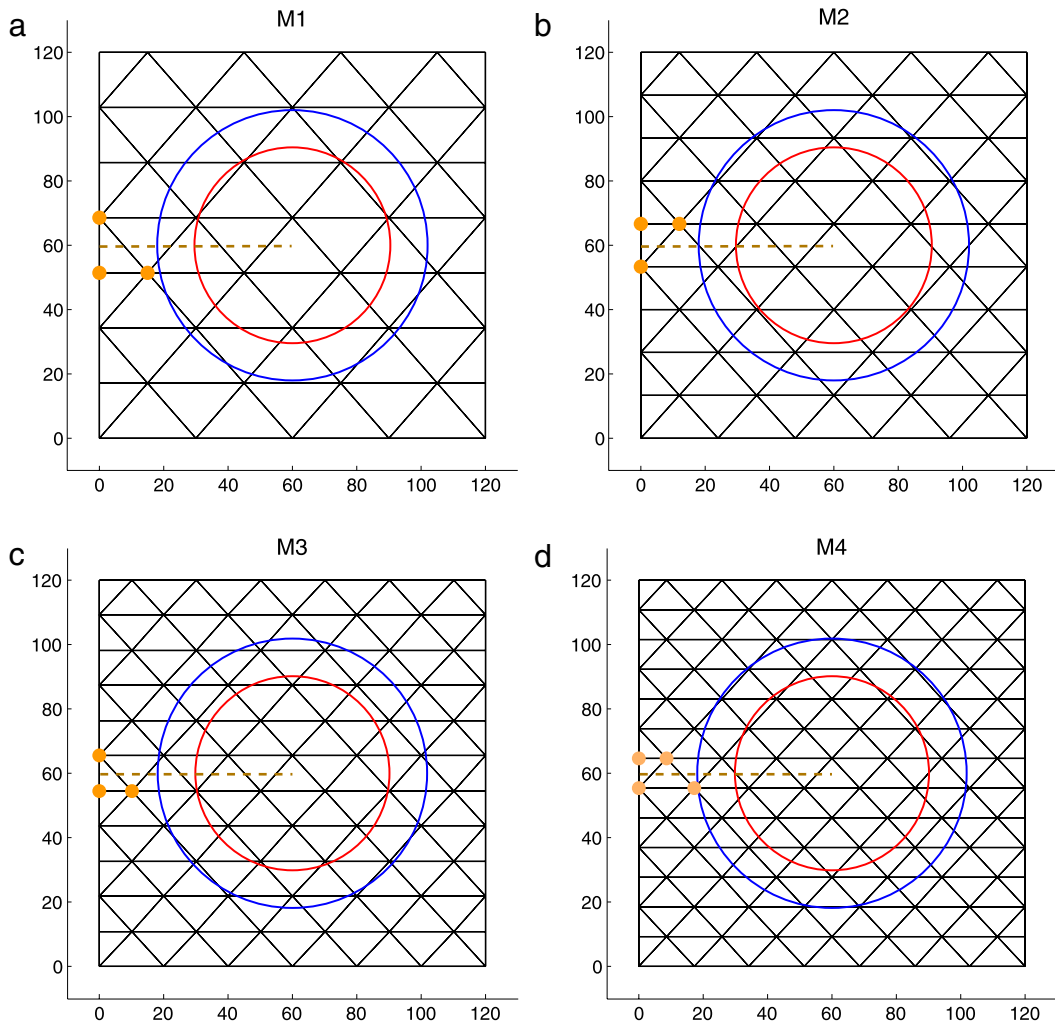


Fig. 3. Discretizations for which the crack cuts elements, with  $\Gamma_C = [0, 60] \times \{60\}$ , such that the crack tip falls inside an element (the crack is along the dashed brown line). Singular enrichment functions (6) are applied according to the geometric pattern. Polynomial enrichment functions (5) are uniformly applied along the domain. (For interpretation of the references to color in this figure, the reader is referred to the web version of this article.)

Additionally, for line integrations, 26 Gauss points were used along each element edge. It is worth noting that this number of integration points is used here only for the sake of evaluation, to separate errors due to numerical integrations from other sources of errors. It should be noted that a routine analysis could use a much smaller number of integration points.

Thus, only one quadrature rule was used for each mesh, independently of the  $p$ -enrichment applied, the pattern of singular enrichments used, and the regularity considered.

The accuracy of the numerical domain integration rules used in the computations of the global stiffness matrices and in the postprocessing is high enough to guarantee the results presented herein. For such evaluation, the numerically integrated strain energies through the analytical stress and strain fields [73,58] were compared with the exact value (10).

Notably, in the case of crack opening over element edges, when there is an entire cloud around the crack tip, Fig. 4(b), a great numerical integration accuracy is achieved, with relative error in terms of strain energy on the order of  $10^{-13}$  or lower.

On the other hand, for the case of crack cutting elements, the numerical integration adopted does not provide so good results, with relative errors on the order of  $10^{-8}$ . Although for the meshes of Fig. 3 there are integration points

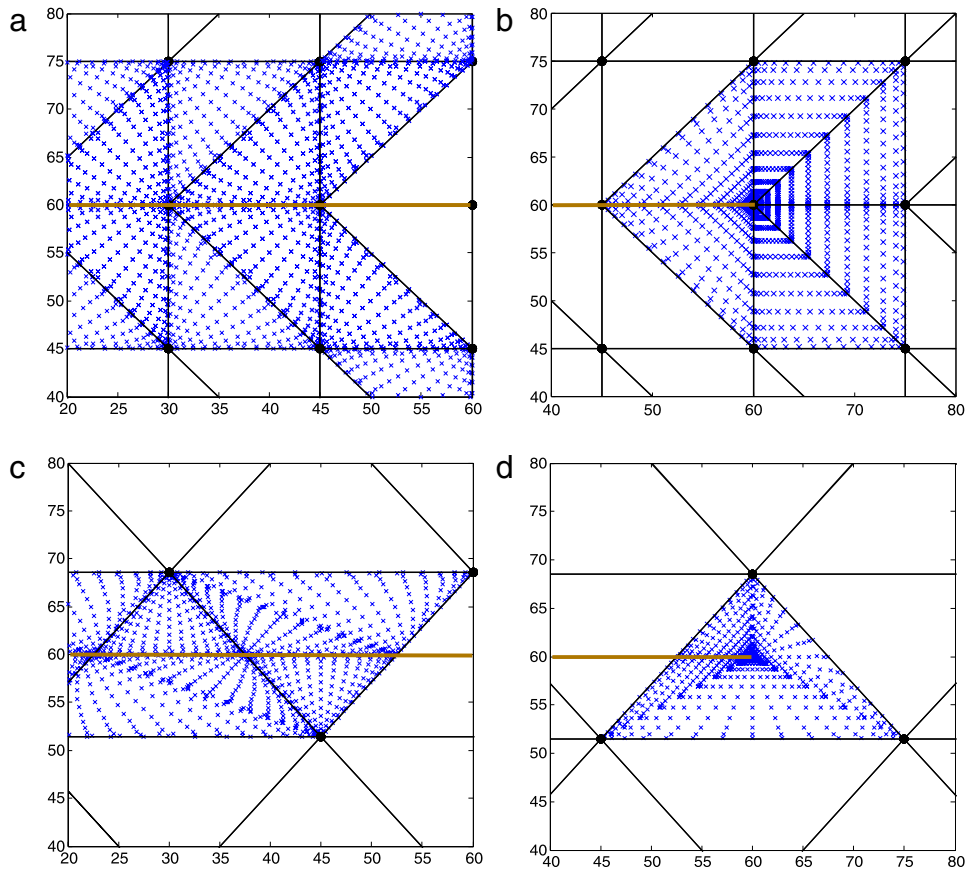


Fig. 4. Quadrature rules employed for domain integrals. (a) Integration on elements free of discontinuity and singularity using Wandzura's triangular quadrature rule [72] with 175 points. (b) Integration on elements around the crack tip when it falls at a node using a special  $15 \times 15$  points quadrature combining the quasi-polar mapping, combined with the quarter-point mapping to move the points toward the crack tip. (c) Integration on elements fully cut by the crack, using Wandzura's rule in the subcells. (d) Integration on the element with the crack tip, considering four subcells on which the quasi-polar/quarter-point combined quadrature is used. The crack line is represented by the brown line.

likely closer to the crack tip (see the situation shown in Fig. 4(d) which occurs for the meshes of Fig. 3) if compared to the points distribution used for the meshes of Fig. 2 (see Fig. 4(b)), the global strain energy integration is not so properly conducted, possibly due to deleterious effects on the first layer of elements around the one that contains the crack tip. Such elements do not contain the crack tip, but they can be still near the perturbed region and would require further special care in order to reduce numerical integration errors.

Therefore, the motivation for paying this high integration cost is to seek a level of accuracy<sup>4</sup> in the computations that would permit comparing  $C^0$  and  $C^k$  discretizations focusing only on the effects of regularity.

### 5.1.2. Convergence in terms of global values

In this work, convergence analysis in terms of global quantities are presented. Additional investigations of the local quality of stress fields around singularities, through the assessment of stress intensity factors, using configurational mechanics (see [74], for instance), will be shown in a forthcoming paper.

<sup>4</sup> An example evaluation has been performed aiming to verify the accuracy level obtained considering a simpler integration procedure. For this, the case with crack cutting elements, for the mesh M2 (like that of Fig. 3), was considered and the Wandzura's triangle integration rule with 175 points was directly applied to the elements crossed by the crack and for that element containing the crack tip, without the subdivision in integration cells. In other words, only the Wandzura's rule was applied to all elements. In this evaluation, the integration error is about  $10^{-3}$ , therefore much higher than the discretization errors in most of the tested cases and, consequently, a considerable amount of the present results would be compromised. From this result, it becomes clear that the numerical integration is an issue of extreme importance in case singular enrichments are used.

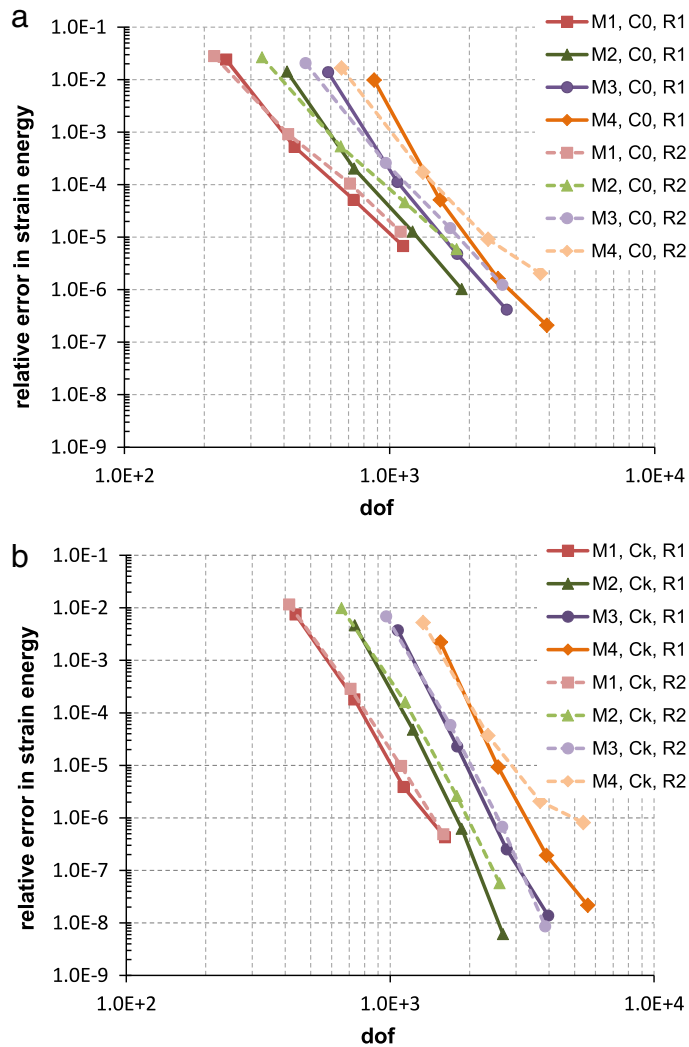


Fig. 5. Convergence  $p$  for the relative error in terms of strain energy for discretizations with crack along element edges, considering the geometric pattern (Fig. 2) of enrichment with branch functions (6) and uniform enrichment with polynomial functions (5). (a)  $C^0$  approximations. (b)  $C^k$  approximations. (For interpretation of the references to color in this figure, the reader is referred to the web version of this article.)

The behavior for different  $C^0$  discretizations, considering  $C^0$  FEM-based PoU's, in terms of strain energy is shown in Fig. 5(a), where the lines correspond to  $p$ -versions for each mesh of Fig. 2, for the two radii employed in the geometric pattern of enrichment. Continuous lines are used for the case of singular enrichment applied inside the R1 circle and dashed lines are used for R2. Uniform polynomial enrichment up to  $p = 3$ , such that  $b = 1, \dots, 4$ , was gradually applied. It is possible to see the algebraic convergence tendency as the elements are reduced, and the initial slopes are more pronounced for more refined meshes as expected.

The decision to display the results against the number of DOF is because the nodes have different number of unknowns and, additionally, because the enrichment pattern undergoes variation in its characteristic dimension. Therefore, graphics with the  $h$ -parameter on the abscissa axis would not be completely appropriate for this study, which is mainly concerned with the effects of regularity, even though the analysis in terms of the  $h$ -parameter is a common practice in the literature (see [7,43], for instance).

In contrast, Fig. 5(b) shows the evolution of the relative error in strain energy for  $C^k$  discretizations, with  $k = \infty$ . Similar to Fig. 5(a), uniform polynomial enrichment was gradually applied up to  $p = 4$ , also resulting in basis degrees  $b = 1, \dots, 4$ . Clearly, it is possible to see higher slopes in Fig. 5(b) for all meshes, mainly in the first segments of the

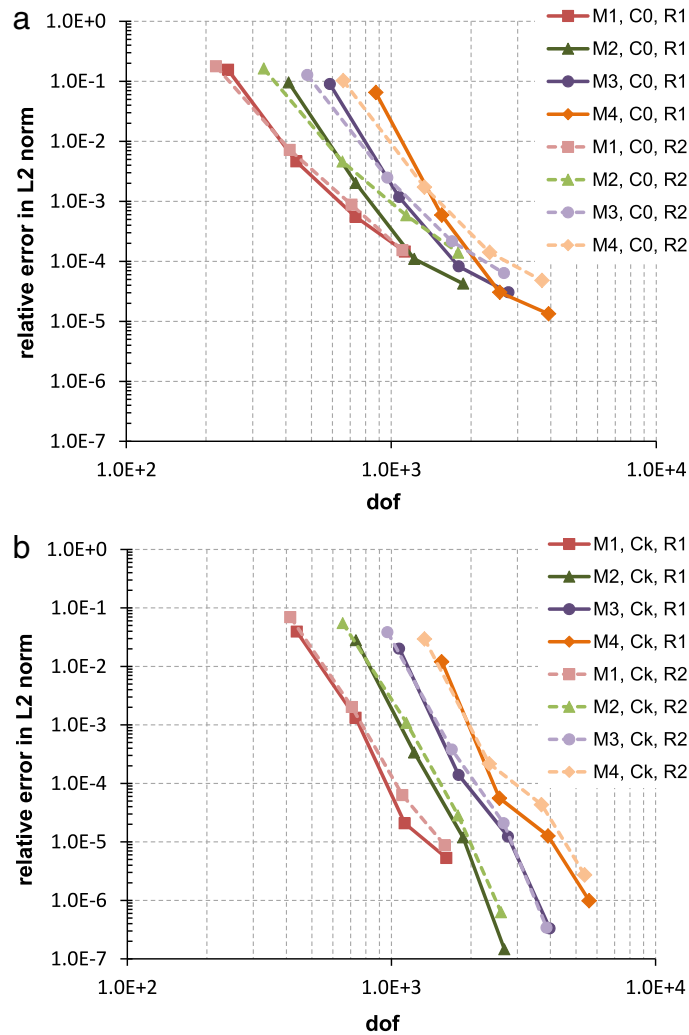


Fig. 6. Convergence  $p$  for the relative error in terms of the  $\mathcal{L}^2$ -norm for discretizations with crack along element edges, considering the geometric pattern (Fig. 2) of enrichment with branch functions (6) and uniform enrichment with polynomial functions (5). (a)  $C^0$  approximations. (b)  $C^k$  approximations. (For interpretation of the references to color in this figure, the reader is referred to the web version of this article.)

curves, compared to the  $C^0$  approximations. Unlike the  $C^0$  case, the dashed lines (relative to R2, the smaller radius of the geometric enrichment pattern) in Fig. 5(b) have slopes very similar to the slopes of the continuous lines (relative to R1, larger radius). This fact indicates the lower sensitivity in the rates of convergence for smooth approximations in face of the reduction of the radius that defines the geometric pattern of enrichment.

Similarly, the relative error in terms of the  $\mathcal{L}^2$ -norm of displacement field is shown in Figs. 6(a) and 6(b) for the  $C^0$  and  $C^\infty$  approximations, respectively. The same features observed in Fig. 5 can be seen here, with regard to the slopes and its almost preservation, independently of the reduction of the enriched zone for  $C^\infty$  models.

For the case of crack cutting elements, Fig. 7 displays the evolution of relative error in terms of strain energy. Again, it can be noted that smooth approximations converge at higher rates compared to the  $C^0$  discretizations, but the indifference of the rate with respect to the way the enrichment is performed is more noticeable. The independence with regard to the dimension of the portion enriched with singular functions becomes more evident as all the curves in Fig. 7(b) are practically superposed for each radius.

Nevertheless, more DOFs are consumed in the case of full  $C^\infty$  discretizations because, for a given error level, the number of unknowns for  $C^k$  discretization is larger than for the corresponding  $C^0$  model. This cost effect is a

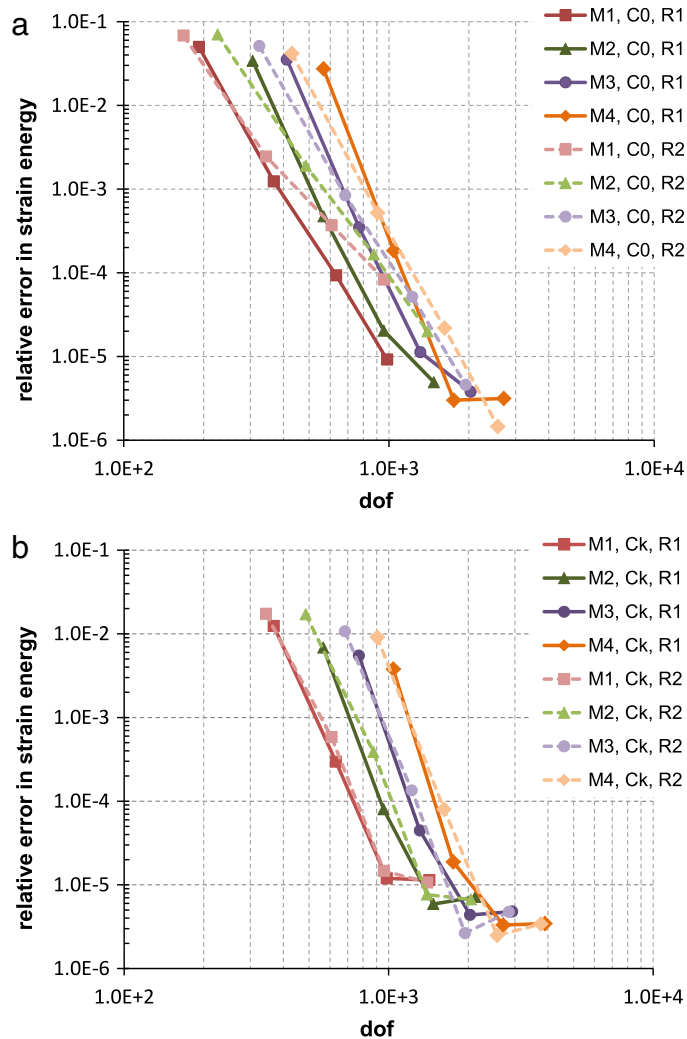


Fig. 7. Convergence  $p$  for relative error in terms of strain energy for discretizations with crack cutting elements, considering the geometric pattern (Fig. 3) of enrichment with branch functions (6) and uniform enrichment with polynomial functions (5). (a)  $C^0$  approximations. (b)  $C^k$  approximations. (For interpretation of the references to color in this figure, the reader is referred to the web version of this article.)

consequence of the lower reproducibility of the smooth PoU, but it can be easily overcome by the simple artifice of applying  $C^k$  functions only where they are beneficial, that is, in the crack vicinity instead of over the entire domain.

It is important to note that there is a saturation of the relative error about the range  $10^{-6}$  which is more evident for the smooth discretizations. The numerical integration errors for the cases in which the crack intersects elements, as commented in the Section 5.1.1, are most likely responsible for this behavior. It is true that some additional care with integration would be necessary to verify this effect but, considering that the influence of regularity on the dependence on the pattern of enrichment can be already seen for this level of accuracy, the quadrature rules cited in Section 5.1.1 are acceptable for the purposes drawn herein.

Considering only these results on convergence in terms of strain energy and  $\mathcal{L}^2$ -norm, for the geometric pattern of enrichment, the advantage of using smooth PoU's could be not so expressive. Therefore, this behavior of the  $C^\infty$  approximations indicates that it could be convenient to consider the topologic pattern of enrichments again, even though it is contrary to the recommendations in the literature. This investigation is necessary to better measure the effects of smoothness in the vicinity of singularities introduced by enrichment. This experiment is also reported along the paper.

### 5.1.3. Conditioning in the geometric pattern

The investigation of the effects on conditioning of stiffness matrices generated from discretizations with different types of PoU functions is necessary to verify the stability of the formulations. First of all, it should be remembered that conventional  $C^0$ -GFEM/XFEM causes singular matrices if polynomial enrichment is used, because both the FEM-based PoU functions and enrichments are polynomials, and therefore a linear dependence occurs [24,46,45,75]. From this observation, the following definition for the condition number is necessary in order to compare  $C^0$  and  $C^k$  approximations

$$\text{cond. number} = \frac{\lambda_M}{\lambda_m} \quad (14)$$

where  $\lambda_M$  is the larger eigenvalue and  $\lambda_m$  is the smaller nonzero eigenvalue.

Although  $C^k$ -GFEM does not lead to singular stiffness matrices in presence of polynomial enrichments, as the PoU functions are not polynomial, the iterative procedure of Babuška [24], applied with the Jacobi preconditioner, was used in this work for both the  $C^0$  and  $C^k$ -GFEM implementations, following [27,28]. The range of perturbation parameters used is  $10^{-10} \leq \varepsilon \leq 10^{-8}$  and the specified tolerance is  $\text{tol} = 10^{-12}$ . In the most evaluations, the convergence is reached in one or two iterations. It can be useful to know that some adjustment in these parameters is necessary in case of to use less accurate numerical integration than those employed herein.

The evolution of the condition number computed according to (14) for  $p$ -version on the discretizations in Figs. 2 and 3 is shown in Figs. 8 and 9, respectively. The results shown in Figs. 8 and 9 are condition numbers computed after enforcement of essential boundary conditions and before the Jacobi pre-conditioner, used with the Babuška procedure [24].

Notably, the condition number for each  $C^k$ -GFEM discretization is higher than its  $C^0$  counterpart with the same number of DOF, even for lower  $b$  degrees.

However, from Fig. 9(b) it may be observed that the conditioning for smooth approximations increases at smaller rates between lower  $b$ -degrees in case of crack cutting elements (Fig. 3), compared to cases with crack over element edges (Fig. 8(b)). In case of  $C^0$  approximations, Fig. 9(a), the condition numbers relative to lower  $b$ -degrees are always higher than the condition number in Fig. 8(a). Additionally, the number of DOF in the case of cracks cutting elements (Fig. 3) is lower than the number of DOF for all polynomial degrees applied on the meshes of Fig. 2. Perhaps the reason for this effect is that the transition zone for the meshes in Fig. 3 is wider than the transition zone for the meshes in Fig. 2.

Evaluating the slopes of the segments between two  $b$ -degrees, considering similar variations in the number of DOF, the rates for  $C^k$  discretizations are slightly higher than for  $C^0$  models. Considering only this type of analysis, it could be suggested that such an effect on the conditioning depends on the regularity of the functions.

To better understand this phenomenon, the distributions of eigenvalues against magnitude order are plotted in Figs. 10 and 11, where the number of occurrences is shown for different orders of magnitude. For such analysis, the mesh M1 of Fig. 2 and the mesh M1 of Fig. 3 are considered, for the case of geometric enrichment with branch functions and uniform polynomial enrichment. In these figures, dashed lines are used for  $C^0$  approximations and continuous lines are used for their  $C^k$  counterparts.

It can be seen that the higher eigenvalues occur in the same quantity for all degrees of polynomial enrichment, for each type of regularity (whose values are displayed in the boxes), and therefore they could be related to some feature common to all degrees of polynomial enrichment: the singular enrichment (or branch functions (6)). Moreover, it is expected that the higher eigenvalues are physically related to deformation modes with higher strain energy content, which are related to the crack tip enrichment functions, because the singular stress and strain fields involved.

Another observation is that the magnitude of the higher eigenvalues for the  $C^k$  approximation is higher than the corresponding values for the  $C^0$  version, possibly as a consequence of the effect exerted by the flat top property of smooth PoU functions, meaning that more information from the branch enrichment functions is captured. Some advantage in terms of good reproduction of the enrichments of the flat-top-featured PoU functions has also been reported in [48,45].

For instance, in Fig. 10(a) the continuous red line and the dashed green line, that correspond to  $C^k b = 1$  and  $C^0 b = 2$  respectively, show that the dispersion of eigenvalues is very similar for matrices of the same dimension,

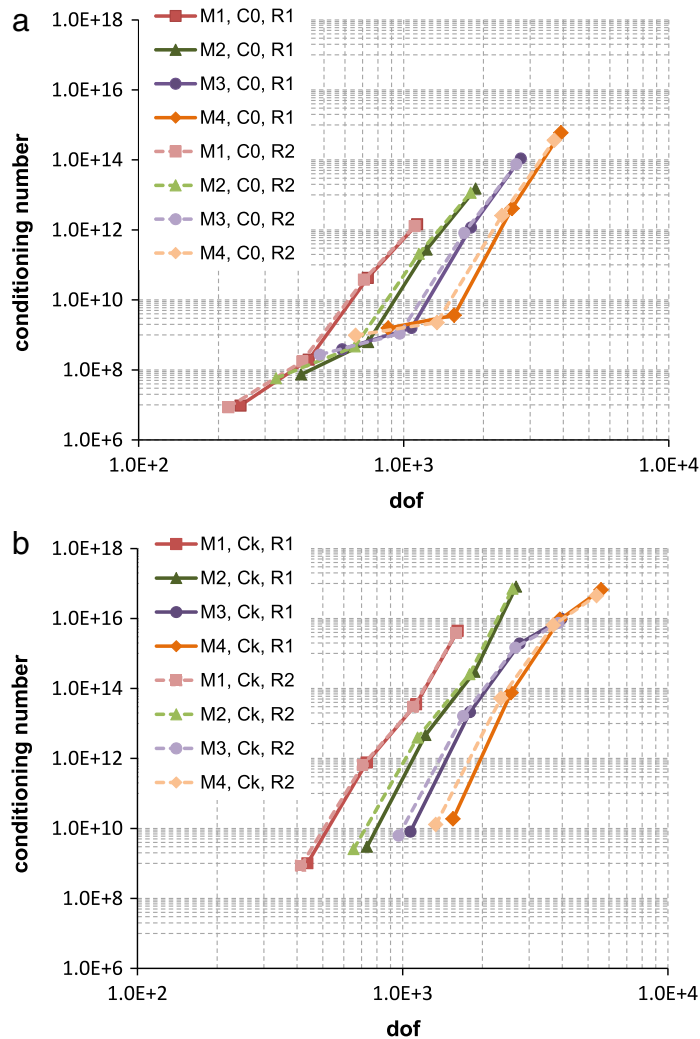


Fig. 8. Evolution of condition number (14) for discretizations with crack along element edges, considering the geometric pattern (Fig. 2) of enrichment with branch functions (6) and uniform enrichment with polynomial functions (5). Condition numbers computed after imposing essential boundary conditions and before the iterative solver proposed by Babuška, with Jacobi preconditioner [24]. Each point is related to a polynomial degree  $b$  of reproducibility. (a)  $C^0$  approximations. (b)  $C^k$  approximations. (For interpretation of the references to color in this figure, the reader is referred to the web version of this article.)

independently of the smoothness of the basis. This conclusion can be reached for other pairs of discretizations with the same number of DOF.

Another possible observation from Figs. 10(a) and 10(b) is that the magnitude of the smaller eigenvalue (smaller nonzero eigenvalue, in the case of  $C^0$  models) decreases as the degree  $b$  of the basis increases. Additionally, the number of occurrences of small eigenvalues increases for higher degrees  $b$ . In other words, the difference between the lines for different degrees  $b$  is observed as the abscissa coordinate is reduced regardless of the smoothness of the PoU functions.

In this way, it could be argued that the higher eigenvalues are related to the crack tip enrichments whereas the lower eigenvalues are related to the specific type of polynomial enrichment used. Therefore, to attribute causality, it should be noted that singular enrichment over smooth PoU produces increasingly higher eigenvalues (see right end in Fig. 10(a)). Consequently, these increasingly higher eigenvalues from  $C^k$ -GFEM will cause higher condition numbers in presence of increasingly smaller eigenvalues produced by polynomial enrichments as in (5).

It should be remarked that, in contrast to the hierarchic FE shape functions commonly used in conventional  $p$ -refinement in FEM, the higher  $b$ -degrees here are related to the smaller eigenvalues. Such hierarchic shape

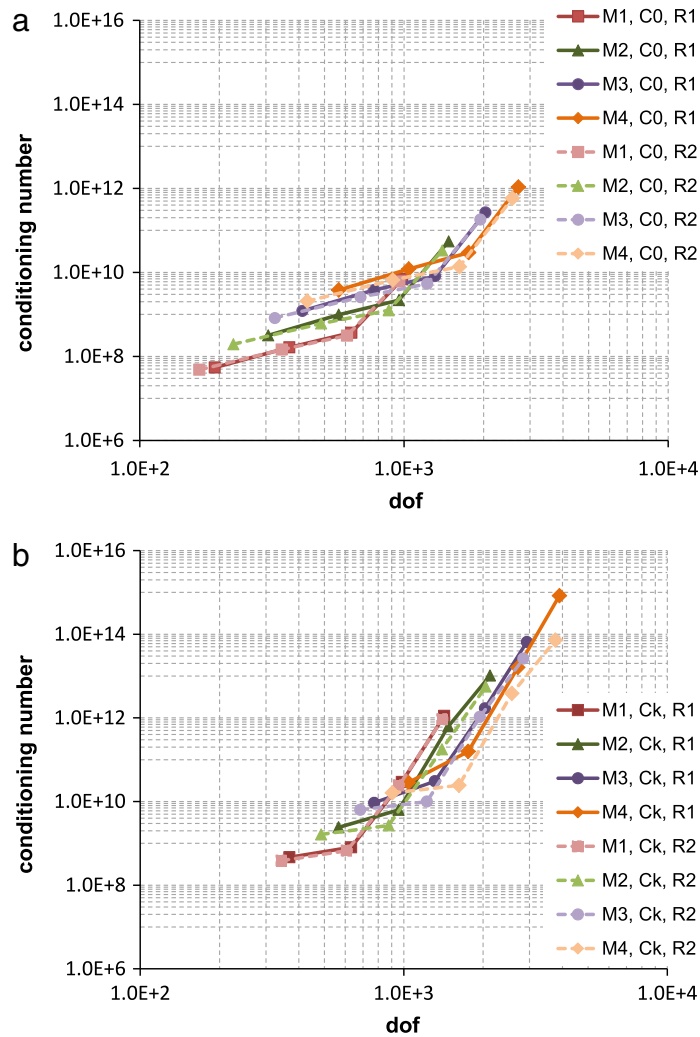


Fig. 9. Evolution of condition number (14) for discretizations with crack cutting elements, considering the geometric pattern (Fig. 3) of enrichment with branch functions (6) and uniform enrichment with polynomial functions (5). Condition numbers computed after imposing essential boundary conditions and before the iterative solver proposed by Babuška, with Jacobi preconditioner [24]. Each point is related to a polynomial degree  $b$  of reproducibility. (a)  $C^0$  approximations. (b)  $C^k$  approximations. (For interpretation of the references to color in this figure, the reader is referred to the web version of this article.)

functions [76] are highly oscillatory and, consequently, they have derivatives that lead to eigenmodes with more strain energy content compared to the  $p$  enrichment functions usually applied in GFEM implementations, as those in (5) (see [24,51,26], for instance). Those monomials are translated and scaled for each cloud in such a fashion that they are null or almost zero over increasing neighborhoods around the associated node, inside its own cloud, as the enrichment degree  $p$  increases.

The increasing condition number is mainly related to the polynomial enrichment employed. From Figs. 10 and 11 it can be seen that for all polynomial enriched  $C^0$  approximations,  $b = 2, 3$  and 4, there are null eigenvalues, which appears at the left end of the horizontal axis. It is also possible to realize that some very small eigenvalues occur for  $C^k$  PoU based approximations, causing a numerical near-linear dependence on the stiffness matrix. The specific type of polynomial enrichment used herein can deteriorate the conditioning, even for smooth approximations that would not generate linear dependence, as the  $C^k$  PoU is not polynomial. This fact justifies the use of the Babuška iterative solver, using Jacobi preconditioner, for the  $C^k$ -GFEM as well as it has been considered by the present authors in [27,28], even for regular problems.

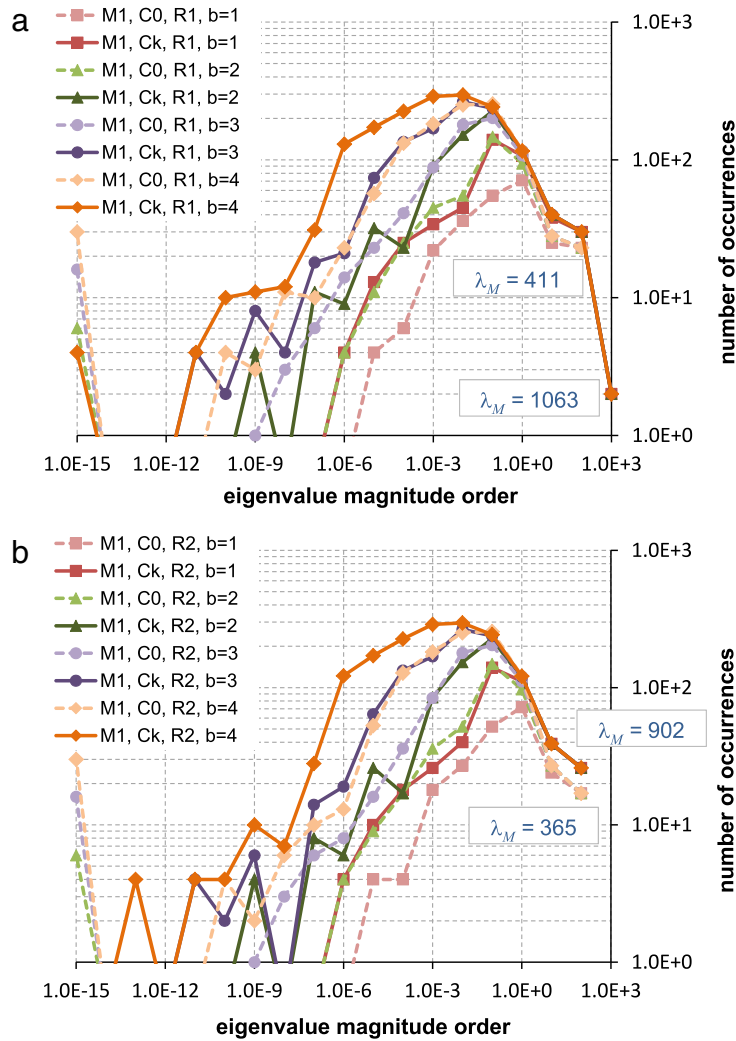


Fig. 10. Distribution of eigenvalues according to their magnitude order for the M1 discretization with geometric pattern of enrichment with crack over element edges (Fig. 2(a)). Each curve corresponds to a specific degree  $b$  of uniform polynomial reproducibility. (a) Singular enrichment zone with radius R1. (b) Singular enrichment zone with radius R2. (For interpretation of the references to color in this figure, the reader is referred to the web version of this article.)

In other words, quasi-singular stiffness matrices can be obtained with  $C^k$ -GFEM when higher-degree polynomial enrichments, with the same nature as in (5), are uniformly applied on the domain, even though linear dependence theoretically does not occur when the PoU functions are not polynomial [24,46,45,48,75]. However, such intense conditioning deterioration related to the polynomial enrichment does not occur when the enrichment is localized, as in adaptive procedures [2,3].

Moreover, the cost associated with the additional DOF necessary to improve reproducibility (as explained in Section 3, in the definition of the reproducibility degree  $b$ ), along with some harmful effects on conditioning, can be minimized by applying smooth PoU functions only near the singularity, where they are more useful. The present authors continue their research on the effects of varying the smoothness along the domain and further results will be shown in a forthcoming paper.

Up to this point, the impact on conditioning has been the remarkable difference between the two types of PoU functions. It is worth noting that for a given polynomial degree of reproducibility  $b$  the smooth version of GFEM requires more unknowns per node than the conventional  $C^0$  counterpart. In general, the geometric pattern of singular

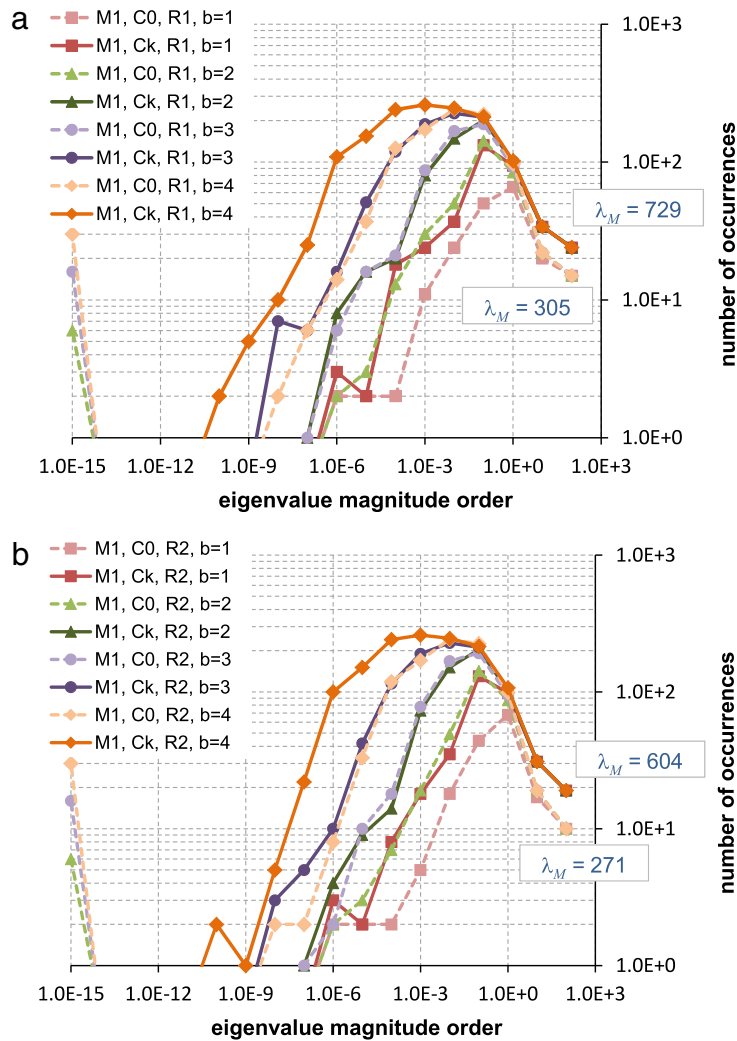


Fig. 11. Distribution of eigenvalues according to their magnitude order for the M1 discretization with geometric pattern of enrichment with crack cutting elements (Fig. 3(a)). Each curve corresponds to a specific degree  $b$  of uniform polynomial reproducibility. (a) Singular enrichment zone with radius R1. (b) Singular enrichment zone with radius R2. (For interpretation of the references to color in this figure, the reader is referred to the web version of this article.)

enrichment is computationally more expensive than the topologic pattern for both  $C^k$  and  $C^0$  frameworks. Therefore, it is opportune to verify if higher regularity would be beneficial in the case of a topologic pattern of enrichment.

The following examples consider the topologic pattern of enrichment with branch functions to reduce the computational cost associated with DOF, and to investigate a probable insensitivity to the pattern of enrichment, as was detected from the results obtained in the case of reducing the radius of geometric enrichment (Figs. 5 to 7).

### 5.2. Topologic pattern of enrichment

The topologic enrichment pattern is the most versatile enrichment pattern in terms of its easiest selection of nodes and smaller number of DOF generated in comparison to the geometric pattern. Because the early results with  $C^k$ -GFEM using singular enrichments have suggested less dependence on the way such enrichment is performed, it is opportune to reconsider the topologic pattern even if this approach has not usually been advisable due to its poorer behavior in terms of convergence verified for  $C^0$ -GFEM/XFEM.

This experiment can provide better information about the effects of higher regularity around a singularity introduced by extrinsically enriched methods. For this purpose, the meshes displayed in Figs. 12 and 13 are considered.

The essential boundary conditions applied here are the same as the ones used for the two sets of meshes considered early for the geometric pattern.

In the former set of meshes, Fig. 12, the crack opens over element edges, such that the discontinuity and the singularity are modeled by enriching only the orange nodes with branch functions (6). These discretizations then employ the enrichment pattern for which the minimum amount of nodes has the associated number of unknowns enlarged with singular enrichments, assuring a complete representation of the singularity on the cloud where the crack tip is enclosed.

On the other hand, for the case of crack cutting elements, Fig. 13, the topologic pattern of enrichment is still more severe than the case of meshes in Fig. 12, since the crack tip falls inside an element and there is not a cloud completely enriched with branch functions (6). This situation would be the more inappropriate, as the transition effects are intensified.

Initially, the singular enrichment functions are applied over a discretization with uniform polynomial degree  $b = 1$  along the mesh, i.e., using uniform enrichment degree  $p = 0$  for  $C^0$ -GFEM and uniform  $p = 1$  for  $C^k$ -GFEM. However, to enhance the representation of the Neumann boundary conditions, the topologic pattern of singular enrichment is considered over uniformly enriched  $b = 2$  discretizations, i.e.,  $C^0$  PoU functions with uniform  $p = 1$  polynomial enrichment for the lower regularity case, and  $C^k$  PoU functions with uniform  $p = 2$  polynomial enrichment for the smooth approximations.

Jointly with the singular enrichment, higher-degree polynomial enrichment functions (5) are locally applied to make the transition more flexible and to reduce the deleterious effects of blending elements [62,61]. The additional  $p$ -enrichment functions were applied only on the nodes in the vicinity of the crack tip. Thus, for the meshes in Fig. 12, polynomial functions (5) were applied to the seven nodes of the cloud containing the crack tip whereas for the meshes in Fig. 13 such functions were applied to the three nodes around the tip.

### 5.2.1. Convergence in terms of global values

The behavior in terms of global measures is shown in Figs. 14–16. Fig. 14 simultaneously displays the evolution of the relative error in terms of strain energy against the number of DOF for  $C^0$  and  $C^k$  approximations in the case of crack opening over element edges (meshes of Fig. 12). Dashed lines are used for  $C^0$  and continuous ones for  $C^k$ . The localized polynomial enrichment on the seven nodes of the cloud containing the crack tip was gradually increased up to  $p = 3$  for the former and up to  $p = 4$  for the latter. In this way, for the case of uniform  $b = 1$ , the four points along the lines correspond to localized polynomial enrichments of degrees  $p = \{0, 1, 2, 3\}$  for the  $C^0$  models, whereas for the smooth GFEM they are related to  $p = \{1, 2, 3, 4\}$ . For uniform  $b = 2$ , the sets of localized polynomial degrees are  $p = \{1, 2, 3\}$  for the  $C^0$  approximations and  $p = \{2, 3, 4\}$  for the  $C^k$ -GFEM.

The relative error in terms of the  $\mathcal{L}^2$ -norm of the displacement field is shown in Fig. 15 for the case of crack over element edges. On the other hand, the results in terms of strain energy for crack cutting elements are shown in Fig. 16.

From the results in Fig. 14(a), it is possible to see that neither the localized  $p$  enrichment nor the mesh refinement can reduce the relative error in terms of strain energy to levels lower than  $6 \times 10^{-2}$  in the case of  $C^0$  approximations, considering only the tent PoU functions for the nodes not involved in the topologic pattern of enrichment. Differently, the results for  $C^k$ -GFEM are remarkable for two main reasons. First, even for the poorest  $C^k$  discretization, mesh M1 with  $p = 1$ , the relative error is smaller than all values obtained with  $C^0$  PoU based approximations. Second, for the tested cases, the relative error decreases as the degree of localized  $p$  enrichment is increased because saturation tendency does not occur for smooth approximations.

Another observation is that when connecting the points for the same degrees  $p$ , for the curves of  $C^0$  approximations, the rate of convergence barely improves as the  $h$  parameter decreases. This fact associated to  $C^0$ -GFEM/XFEM models agrees with early observations reported by [7,8], in which convergence rates for the  $h$  version were provided, considering different degrees of shape functions in the standard XFEM framework. This fact has motivated several other researches to employ geometric pattern of enrichment as a means to recover quasi-optimal or optimal convergence rates (see also [77]).

Additionally, for the poorest  $C^k$  discretization in the case of uniform  $b = 2$ , Fig. 14(b), the relative error is smaller than all values for  $C^0$  models, even when the rates of convergence  $C^0$  for the lower regularity approximations are significantly enhanced. It can be seen from Figs. 14(a) and 14(b), separately, that the smooth version of GFEM always provides smaller errors for a given number of DOF.

Similar observations hold for the relative error in terms of the  $\mathcal{L}^2$ -norm of the displacement field, as shown in Fig. 15, and for the relative error in terms of strain energy for crack cutting elements, shown in Fig. 16.

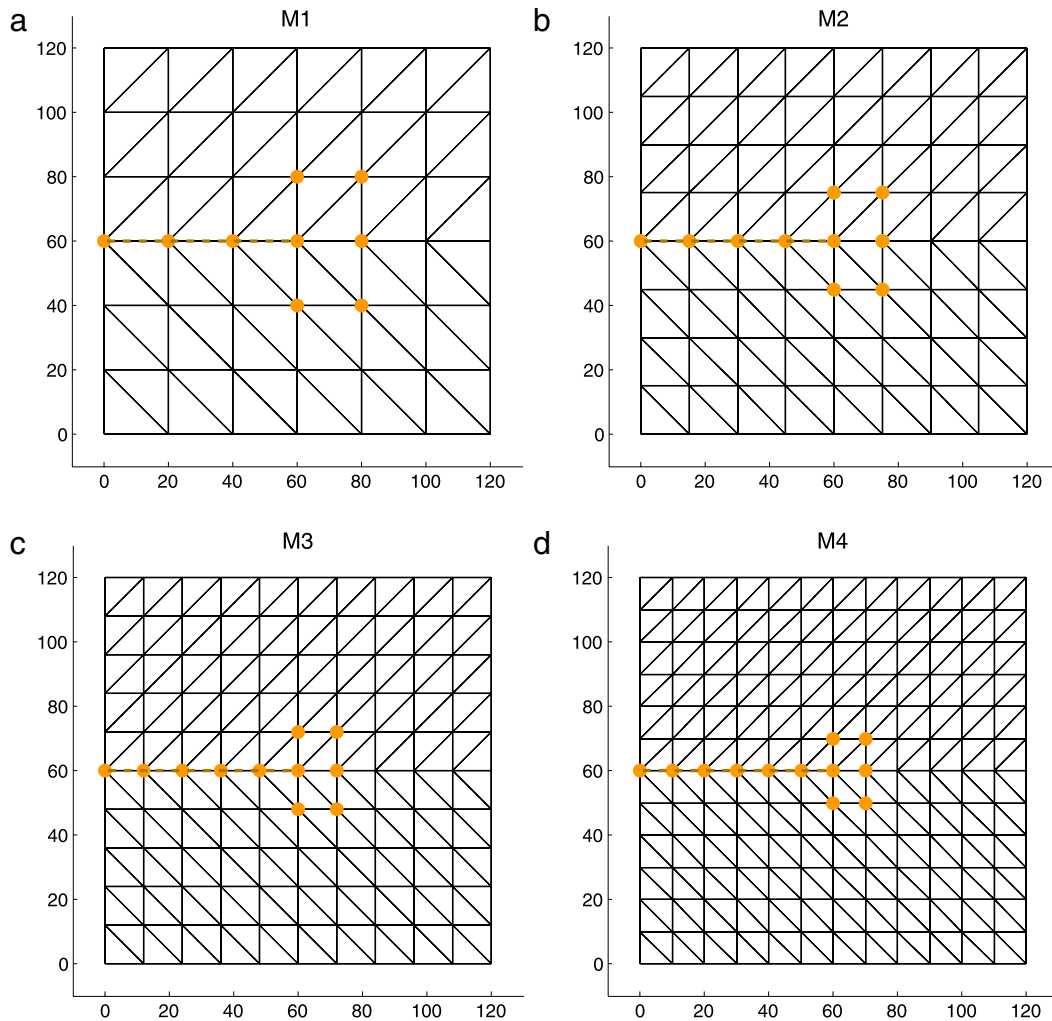


Fig. 12. Discretizations for which the crack opens along element edges, with  $\Gamma_C = [0, 60] \times \{60\}$ , such that the crack tip falls on a node (the crack is along the dashed brown line). Singular enrichment functions (6) are applied according to the topologic pattern. Polynomial enrichment functions (5) are also locally applied on the seven nodes of the cloud containing the crack tip. (For interpretation of the references to color in this figure, the reader is referred to the web version of this article.)

Additionally, the difference between the smaller error for  $C^0$  M1 models and the larger error for  $C^k$  M1 discretizations for the case of crack over element edges, in Fig. 14(a), is similar to the difference seen in Fig. 16(a), for crack cutting elements. This fact may indicate that the superiority of smooth functions is independent on the crack path, in other words, whether the crack cuts elements or not, even in case of topologic enrichment pattern. This conclusion is further supported for uniform degree  $b = 2$  by the results shown in Figs. 14(b) and 16(b).

On the other hand, despite the reproducibility degree  $b$ , it may be argued that the error for  $C^0$  models is smaller than the error for the  $C^k$  counterparts, for the same number of DOF, comparing the Figs. 14(a) and 14(b). For instance, it is possible to see that the error for the mesh M1, using  $b = 2$ , in case of  $C^0$  approximation in Figs. 14(b) is about  $7.0 \cdot 10^{-3}$  whereas for  $b = 1$ , in case of  $C^k$  approximation (Fig. 14(a)), for the same mesh, the error is about  $2.0 \cdot 10^{-2}$ . Nevertheless, it should be cited that the main motivation for considering  $b = 2$  in the experiments with the topologic pattern of enrichment with singular functions is to verify some influence exerted by the Neumann boundary conditions. In other words, considering the  $C^k$  models with  $b = 1$ , the traction boundary conditions are approximated by three functions (for each physical displacement component) at each node along the boundary, whereas in case of  $C^0$  models only one function is employed, that is, the conventional shape function. The  $\mathcal{L}^2$ -norm of the approximated forces on

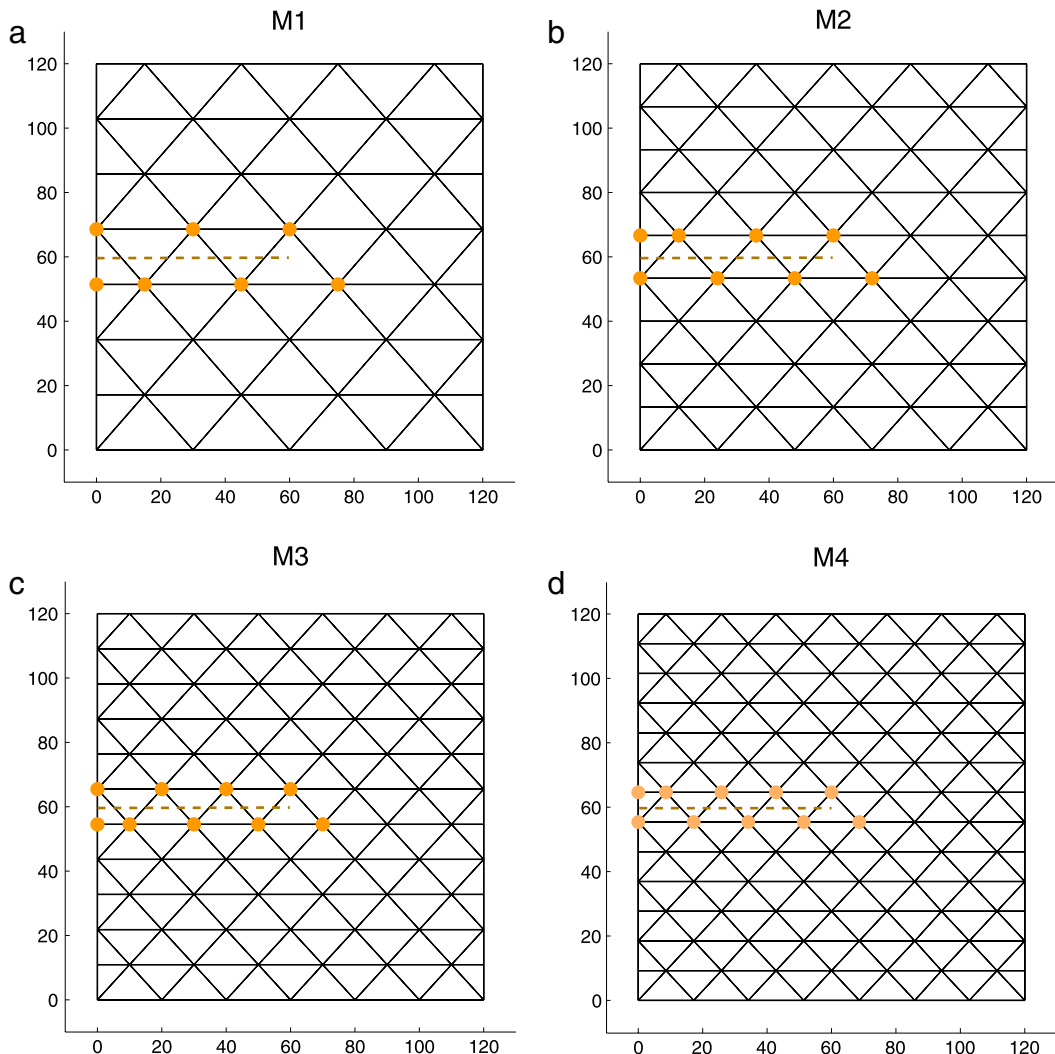


Fig. 13. Discretizations for which the crack cuts elements, with  $\Gamma_C = [0, 60] \times [60]$  such that the crack tip falls inside an element (the crack is along the dashed brown line). Singular enrichment functions (6) are applied according to the topologic pattern. Polynomial enrichment functions (5) are also locally applied on the three nodes around the crack tip. (For interpretation of the references to color in this figure, the reader is referred to the web version of this article.)

the boundary shows the difference between the models with  $b = 1$  and  $b = 2$ . Thus, as there is difference between the applied forces for the models with  $b = 1$  and  $b = 2$ , such a comparison between  $C^k$  and  $C^0$  approximations could not be appropriate, unless the discretization along the Neumann boundary is identical in both cases. Of course, such a difference in the applied forces also occurs in the experiments with the geometric pattern, however, such difference significantly reduces as the  $b$  degree increases up to 4, since the traction boundary condition is smooth.

Additionally, more than pointwise values of error for a given number of DOF, it may be seen that the higher regularity enables to improve the rates of convergence in the presence of mesh refinement for all degrees of localized  $p$  enrichment. Moreover, it should be noted that the accuracy improves as the degree  $b$  increases for both  $C^k$  and  $C^0$  approximations, as expected in this type of Galerkin techniques. Thus, the question of why the use of lower degree GFEM/XFEM, applying only singular (and Heaviside) enrichment functions is so widespread is raised. From the results herein, it is well evident that both  $C^0$  and  $C^k$  approximations for stresses around cracks benefits significantly from polynomial enrichment, even on the neighborhood of the crack tip.

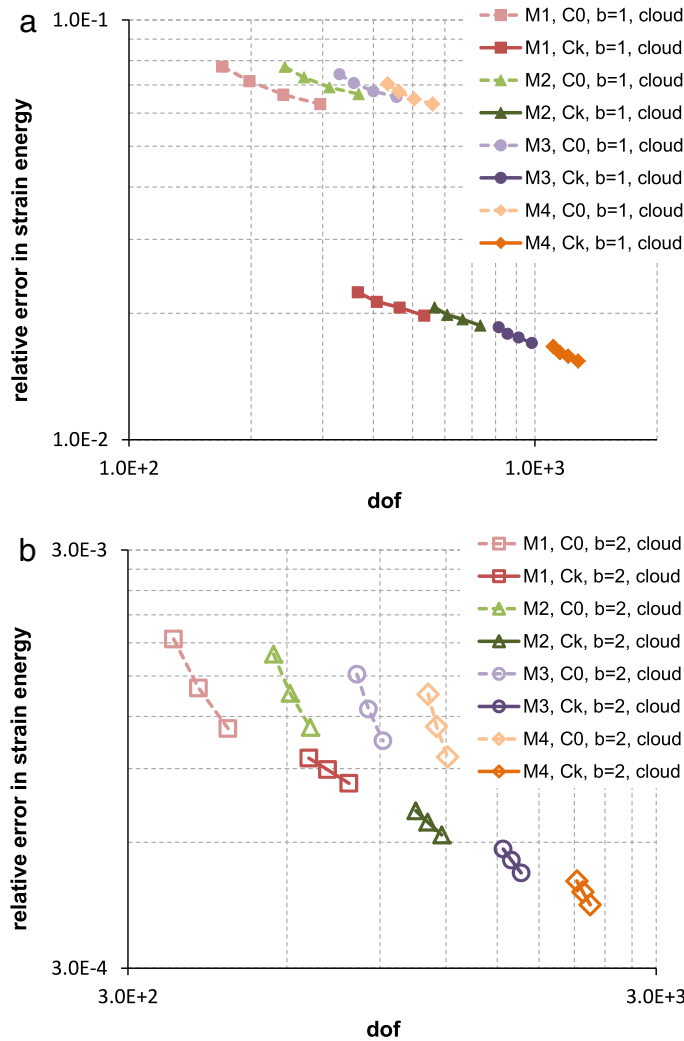


Fig. 14. Convergence  $p$  for relative error in terms of strain energy for discretizations with the crack opening along element edges, considering the topologic pattern (Fig. 12) of enrichment with branch functions (6) and localized enrichment with polynomial functions (5). (a)  $b = 1$  along the remaining part of the domain. (b)  $b = 2$  along the remaining part of the domain. (For interpretation of the references to color in this figure, the reader is referred to the web version of this article.)

The impact of regularity on conditioning, for the topologic pattern of singular enrichment, will now be shown. Similar to the geometric pattern, the evolution of the condition number (14) for the  $p$ -version and some distributions of the eigenvalues are displayed to verify or confirm early observations.

### 5.2.2. Conditioning in the topologic pattern

Fig. 17 shows the evolution of condition numbers for the  $p$ -version on meshes of Fig. 12, where the crack opens over element edges, whereas Fig. 18 shows the behavior in terms of conditioning for discretizations with the crack cutting elements, for the meshes of Fig. 13. The condition number for the smooth GFEM is always larger, and grows at higher rates, than the corresponding to  $C^0$ -GFEM/XFEM.

Eigenvalues distributions are used again to explain the behavior in terms of conditioning. Thus, the number of occurrences for each order of magnitude of eigenvalues are shown in Figs. 19 and 20 for the  $C^0$  and  $C^k$  discretizations, respectively. In these figures, the higher eigenvalues are displayed in the boxes. As previously verified for the geometric pattern of enrichment, the higher eigenvalues in the case of  $C^k$ -GFEM are larger than the higher eigenvalues

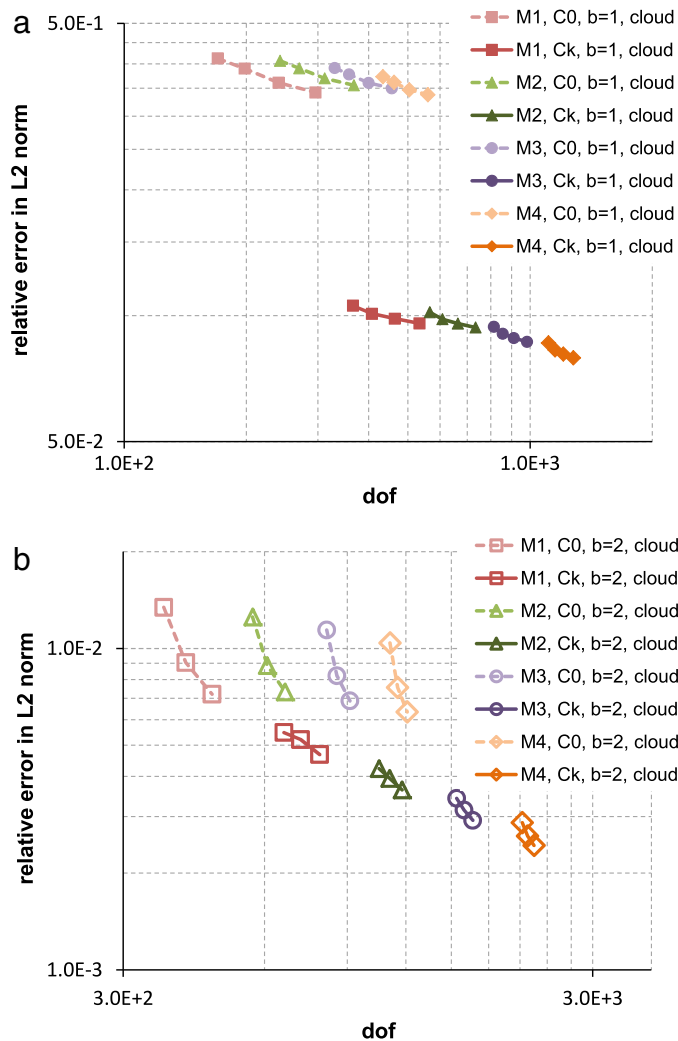


Fig. 15. Convergence  $p$  for relative error in terms of  $L^2$ -norm for discretizations with the crack opening along element edges, considering the topologic pattern (Fig. 12) of enrichment with branch functions (6) and localized enrichment with polynomial functions (5). (a)  $b = 1$  along the remaining part of the domain. (b)  $b = 2$  along the remaining part of the domain. (For interpretation of the references to color in this figure, the reader is referred to the web version of this article.)

for conventional GFEM/ XFEM, and this phenomenon suggests that the flat-top of the smooth PoU functions of  $C^k$ -GFEM is more effective at incorporating the singularity.

Comparing Fig. 18 to Fig. 17 it is possible to see that the condition number, for the case of crack cutting elements, is always higher than those obtained for the discretizations where the crack opens over element edges. Looking at the eigenvalues distributions, it is notes that the higher eigenvalues in Fig. 20 are smaller than the higher eigenvalues in Fig. 19, as expected because no complete cloud is enriched with singular functions in the meshes of Fig. 13. However, the smaller eigenvalues for the case of crack cutting elements are smaller than the correspondents for the crack over element edges (see the dashed red lines in Figs 20(a) and 19(a), for instance). This fact suggests that the deleterious effect of the transition is intensified for the meshes of Fig. 13.

Another important observation is that the higher eigenvalues are the same regardless of whether  $b = 1$  or  $b = 2$  is used, for both situations of crack positioning in relation to the mesh, confirming that such higher eigenvalues are related to the singular enrichment functions.

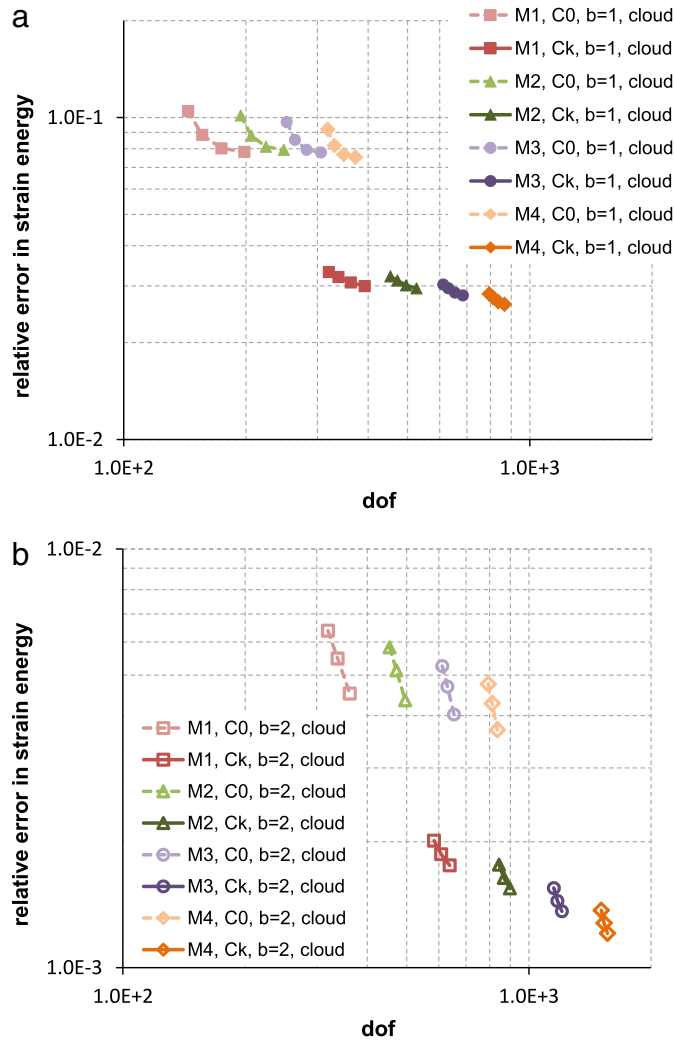


Fig. 16. Convergence  $p$  for relative error in terms of strain energy for discretizations with the crack cutting elements, considering the topologic pattern (Fig. 13) of enrichment with branch functions (6) and localized enrichment with polynomial functions (5). (a)  $b = 1$  along the remaining part of the domain. (b)  $b = 2$  along the remaining part of the domain. (For interpretation of the references to color in this figure, the reader is referred to the web version of this article.)

Finally, it is clear that the conditioning is more perturbed if polynomial enrichment functions, as those in (5), are applied simultaneously with singular enrichments over smooth PoU functions. Nevertheless, the flat-top of  $C^k$  PoU functions allows a more appropriate incorporation of the singularity into the ansatz than the  $C^0$  counterparts, as seen from the eigenvalues distributions. This statement is further supported by comparing the stress fields for both types of approximations. Thus, some fields of exact error in stress are displayed. Fig. 21 shows the exact error in the  $y$ -component of stress for the case of topologic enrichment pattern with crack opening over element edges, for the mesh M2 of Fig. 12. The exact error was chosen because the relative error measure is inviable since there are null exact values along the crack faces. Moreover, a minimum cutoff value of  $1 \times 10^{-10}$  for the radius coordinate was used in order to compute the values at the crack tip. The exact error fields are related to the cases of uniformly applied polynomial enrichment resulting in degrees  $b = 1$  and  $b = 2$ . Thus, these results correspond to the upper points of the curves shown in green in Fig. 14.

Similarly, Fig. 22 displays the exact error in the  $y$ -component of stress for the case of topologic enrichment pattern for crack cutting elements. More specifically, the mesh M2 of Fig. 13 is considered.

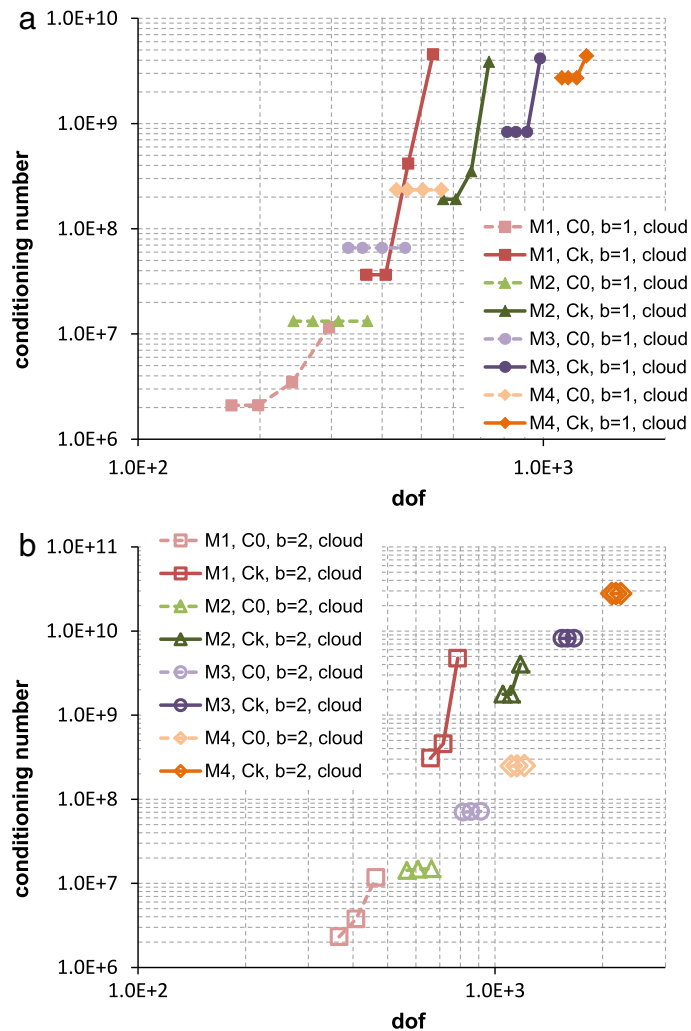


Fig. 17. Evolution of condition number (14) for discretizations with the crack opening along element edges, considering the topologic pattern (Fig. 12) of enrichment with branch functions (5) and localized enrichment with polynomial functions (5). Condition numbers computed after imposing essential boundary conditions and before the iterative solver proposed by Babuška, with Jacobi preconditioner [24]. (a)  $b = 1$  along the remaining part of the domain. (b)  $b = 2$  along the remaining part of the domain. (For interpretation of the references to color in this figure, the reader is referred to the web version of this article.)

From these error fields in terms of stress it is notable how the flat-top of  $C^k$ -GFEM PoU functions improves the singularity representation. In the case of crack opening over element edges, for which there is a cloud completely enriched with branch functions, the error is almost null in the neighborhood of the crack tip (Figs. 21(a) and 21(c)). Furthermore, the error values for smooth approximations are much smaller than for the conventional  $C^0$ -GFEM/XFEM, and such higher error values are less wide-spread as the reproducibility degree  $b$  increases for the  $C^k$ -GFEM.

The good performance of smooth GFEM becomes more evident from the error fields in Fig. 22, where it can be seen that in the case of  $b = 2$  the maximum error values for  $C^k$ -GFEM are approximately five times smaller than the corresponding  $C^0$  model, see Figs. 22(c) and (d). It should be remembered that in the case of topologic pattern of enrichment with crack cutting elements there is no cloud completely enriched with singular functions and thus the transition (blending) effects can be intensified.

Therefore, better stress approximations around the crack tip may be obtained in the case of  $C^k$ -GFEM, even using the enrichment pattern that applies especial enrichment functions to the minimum number of nodes necessary to guarantee the crack representation. The consequence of higher eigenvalues produced in smooth approximations,

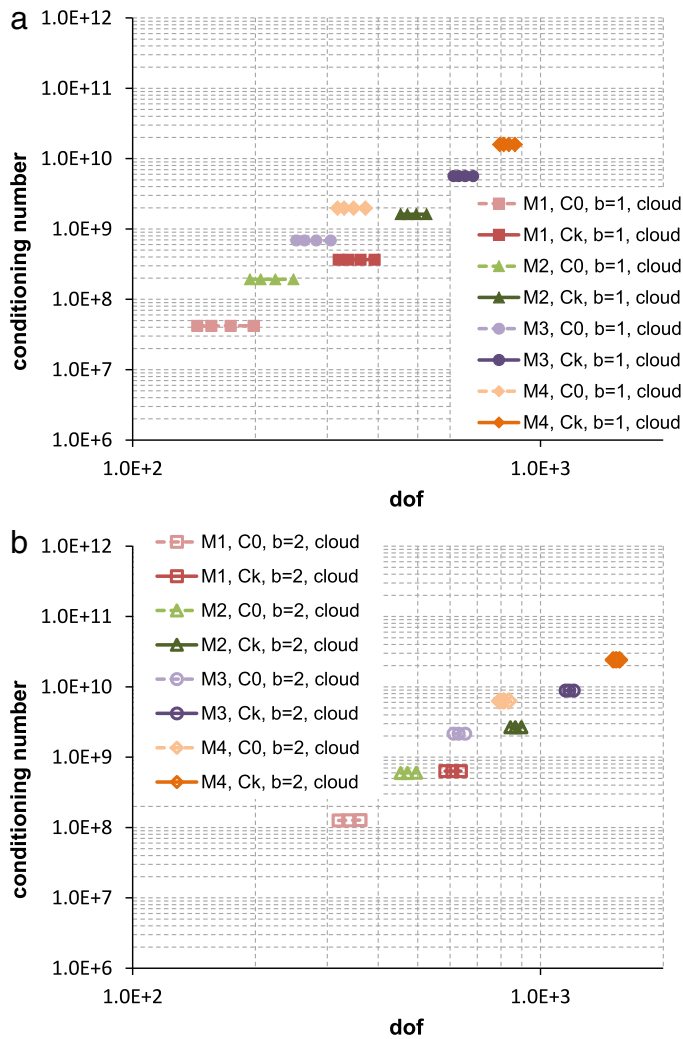


Fig. 18. Evolution of condition number (14) for discretizations with crack cutting elements, considering topologic pattern (Fig. 13) of enrichment with branch functions (5) and localized enrichment with polynomial functions (5). Condition numbers computed after imposing essential boundary conditions and before the iterative solver proposed by Babuška, with Jacobi preconditioner [24]. (a)  $b = 1$  along the remaining part of domain. (b)  $b = 2$  along the remaining part of domain. (For interpretation of the references to color in this figure, the reader is referred to the web version of this article.)

besides the benefits of continuous stress fields around the crack tip, seems to be less deleterious than the effect of polynomial enrichments (5) on the eigenvalues distribution. Moreover, regarding the polynomial enrichment, these findings suggest searching for different types of polynomial enrichment functions, which is also a current research topic for the present authors.

### Concluding remarks

The special instance of the GFEM/XFEM that furnishes smooth approximations,  $C^k$ -GFEM [9], was applied to modeling singular stress fields that occur in problems of two-dimensional LEFM. This methodology, in its original form, enables the construction of arbitrary  $C^k$ -continuous PoU functions for arbitrary polygonal clouds. Remarkably, there is no geometrical restrictions on either the elements or the clouds. Moreover, it is important to cite that an extension to elements with curved edges is possible by using convenient distance functions, such as some of the ones described in [13], as cloud edge functions.

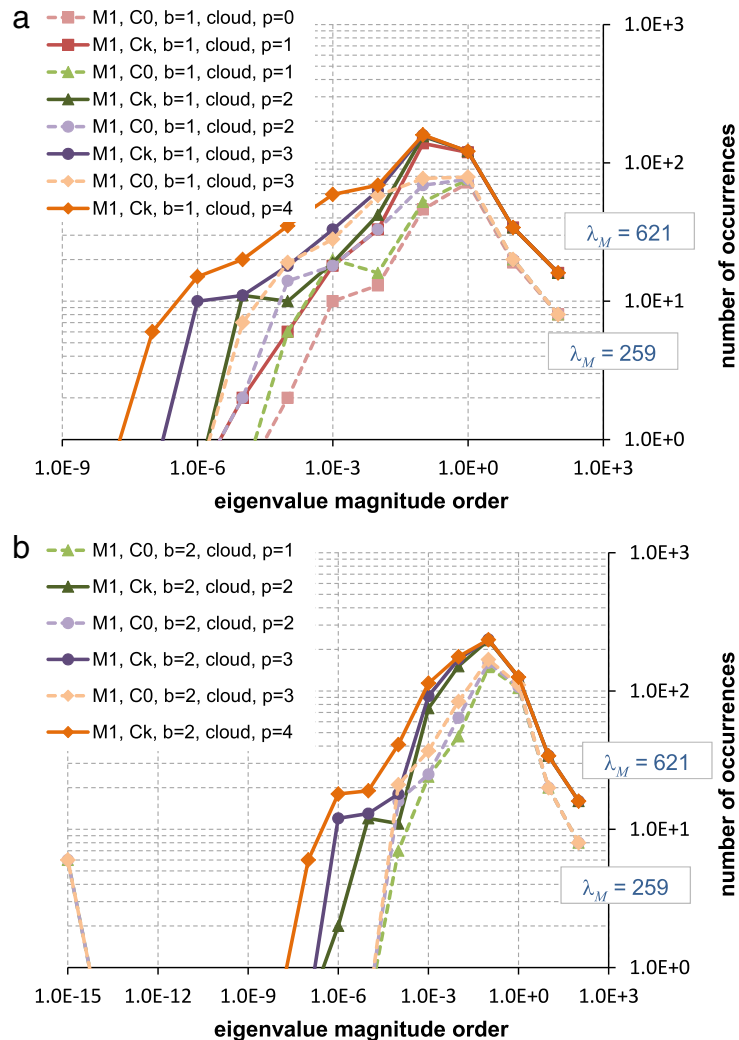


Fig. 19. Distribution of eigenvalues according to their magnitude order for the M1 discretization with the topologic pattern of enrichment with the crack opening over element edges (Fig. 12(a)). Each curve is correspondent to a specific degree  $b$  obtained with locally applied polynomial enrichment. (a)  $b = 1$  along the remaining part of the domain. (b)  $b = 2$  along the remaining part of the domain. (For interpretation of the references to color in this figure, the reader is referred to the web version of this article.)

In summary,  $C^k$ -GFEM is a mesh-based discretization technique that combines higher regularity, the flat-top property, globally defined coordinates, and compact support and could be applied to different geometrical mesh entities (elements and/or clouds). Although its smooth PoU has lower reproducibility than the  $C^0$  PoU one, the extrinsic enrichment, using the same scheme as the  $hp$ -cloud method [21], makes it possible to improve approximation capabilities.

The strain and stress fields are naturally continuous along the element edges without any type of averaging or smoothing post-processing operation, and the method is very robust with regard to severe mesh distortions [27] as all components of the ansatz are defined in global coordinates. Besides the higher-order continuity, the  $C^k$  PoU functions have non-constant derivatives inside the elements which favor capturing much localized features even using coarse meshes [78]. It should be further mentioned that the subroutine for computation of  $C^k$ -GFEM functions can be encapsulated, in such a fashion that the standard displacement based structure of the standard GFEM/XFEM formulations is preserved.

Additionally, some rates of convergence for the  $h$ -version are tabulated for a further comparison. For this purpose, the relative error in the energy norm,  $\|\mathbf{u}\|_E = \sqrt{U(\mathbf{u})}$ , using (9), was considered to compare the obtained rates of

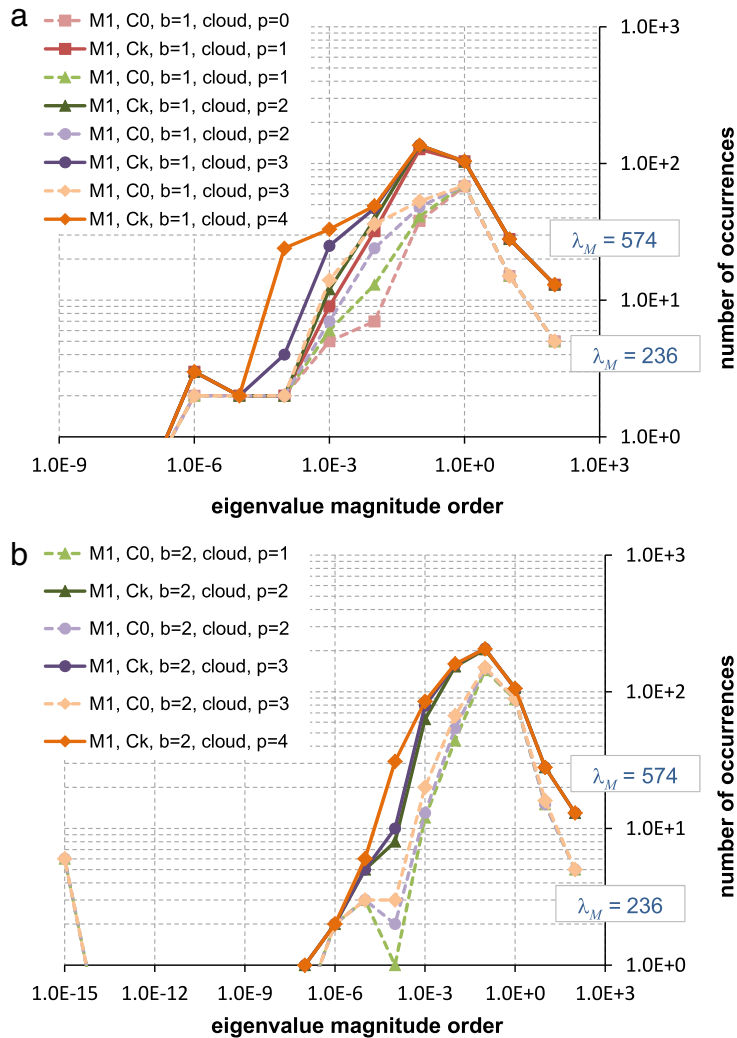


Fig. 20. Distribution of eigenvalues according to their magnitude order for the M1 discretization with the topologic pattern of enrichment with the crack cutting elements (Fig. 12(a)). Each curve is correspondent to a specific degree  $b$  obtained with locally applied polynomial enrichment. (a)  $b = 1$  along the remaining part of the domain. (b)  $b = 2$  along the remaining part of the domain. (For interpretation of the references to color in this figure, the reader is referred to the web version of this article.)

convergence with those theoretical values presented in [76,65] for FEM. It is known that the error is asymptotically approximated by

$$\log \|e\|_E \approx \log C - \beta \log(DOF) \tag{15}$$

where the absolute value  $\beta$  is the asymptotic rate of convergence and  $C$  is a constant. According to [76,65], the model problem studied herein is classified in the B category due to the presence of a singular point inside the domain. Then, the theoretical rate of convergence  $\beta$  for FEM is  $\beta = 1/2 \min(b, \lambda)$ , where  $b$  is the approximation degree and  $\lambda$  is the singularity order, which is  $\lambda = 1/2$  for this problem [58].

According to [7,8], the geometric pattern of enrichment allows the conventional  $C^0$ -GFEM/XFEM to recover optimal rates of convergence, typical of smooth problems (those classified as in the A category, following [76]), for which  $\beta = b/2$ .

Table 1 shows that when singular enrichment functions (6) are applied to the nodes inside the larger radius R1, for the case of crack opening over element edges (Fig. 2), the rates of convergence nearly match the theoretical value for A category in the case of  $b = 2, 3$ , for the  $C^0$  models. In contrast, for the  $C^k$  models, the rate of convergence

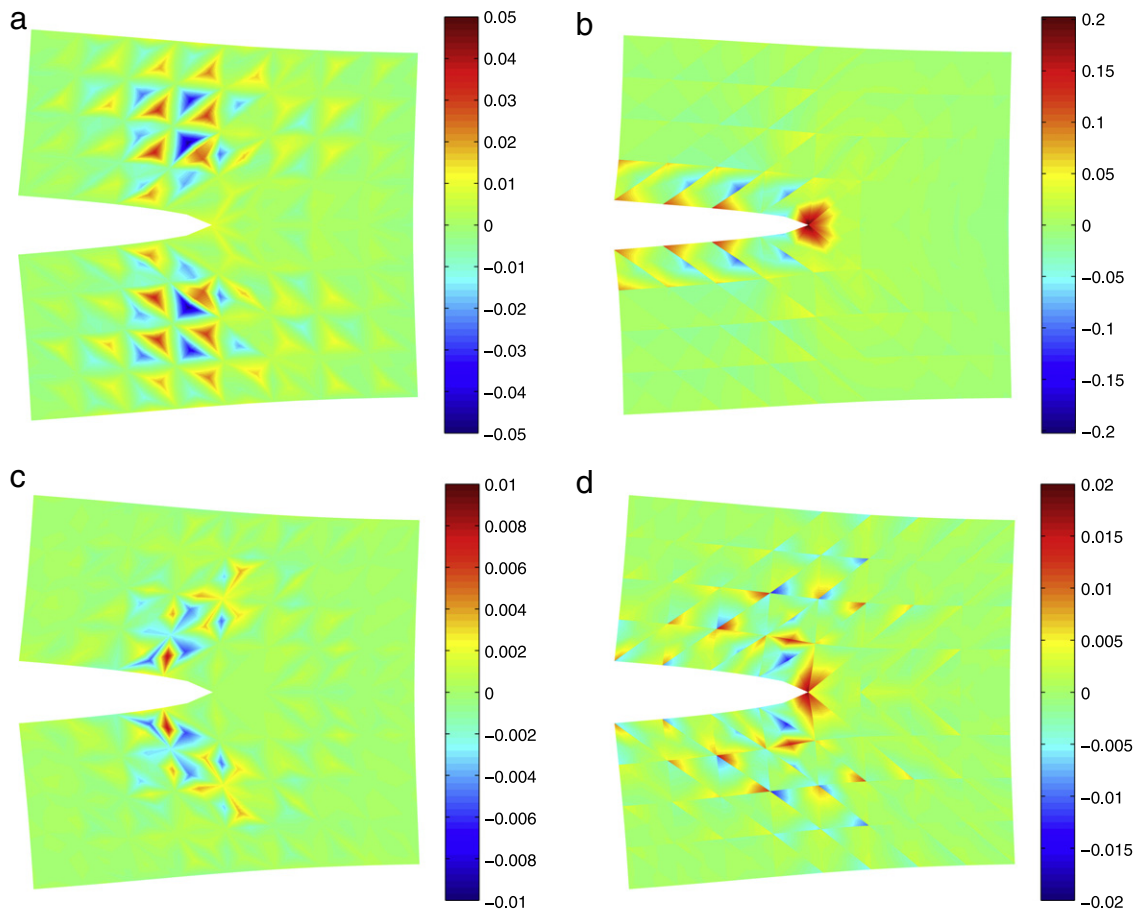


Fig. 21. Exact error for the  $y$ -component of stress. Topologic pattern of enrichment with singular functions (6) over the mesh M2 of Fig. 12. Polynomial enrichment functions (5) uniformly applied along the domain. (a)  $C^k$  approximation with  $b = 1$ . (b)  $C^0$  approximation with  $b = 1$ . (c)  $C^k$  approximation with  $b = 2$ . (d)  $C^0$  approximation with  $b = 2$ .

for  $b = 1$  nearly match the theoretical value for A category while a superconvergent behavior is verified in the case of  $b = 2$ . These facts mean that the geometric pattern of enrichment, with an appropriate radius, is capable of completely removing the singularity of the solution to be approximated. Additionally, smooth PoU functions enable good convergence rates even for lower polynomial degrees.

Table 1 also shows that reducing the radius, i.e., for the radius R2, the rates of convergence for  $C^0$ -GFEM/XFEM are reduced for all degrees  $b$ . On the other hand, for  $C^k$ -GFEM, the rates of convergence are practically preserved in cases of  $b = 1, 2$ , and in cases of  $b = 3, 4$  the sharp reduction may be due to ill conditioning (see dashed orange lines in Figs. 5(b) and 8(b)).

The topologic pattern of singular enrichment over  $C^0$  approximations for the discretizations of Fig. 12, with only localized polynomial enrichments, is almost useless in terms of improving convergence. Even considering uniformly applied polynomial enrichment in case of  $C^0$  approximations, the rates of convergence for the topologic enrichment pattern are much smaller than the theoretical value for B category. In contrast, in the case of smooth approximations with  $b = 1$ , some improvement in terms of convergence rates is still obtained by applying topologic singular enrichment. Moreover, for higher uniform polynomial degree reproducibility,  $b = 2$ , the rates of convergence are slightly higher than the theoretical value for B category.

Therefore, reducing the radius that defines the geometric pattern of enrichment shows the superiority of  $C^k$ -GFEM over  $C^0$ -GFEM/XFEM in terms of its almost independence of convergence rates for the  $p$ -versions regarding the way the singular enrichment is performed. This feature is more visible in the case of topologic pattern of enrichment, when

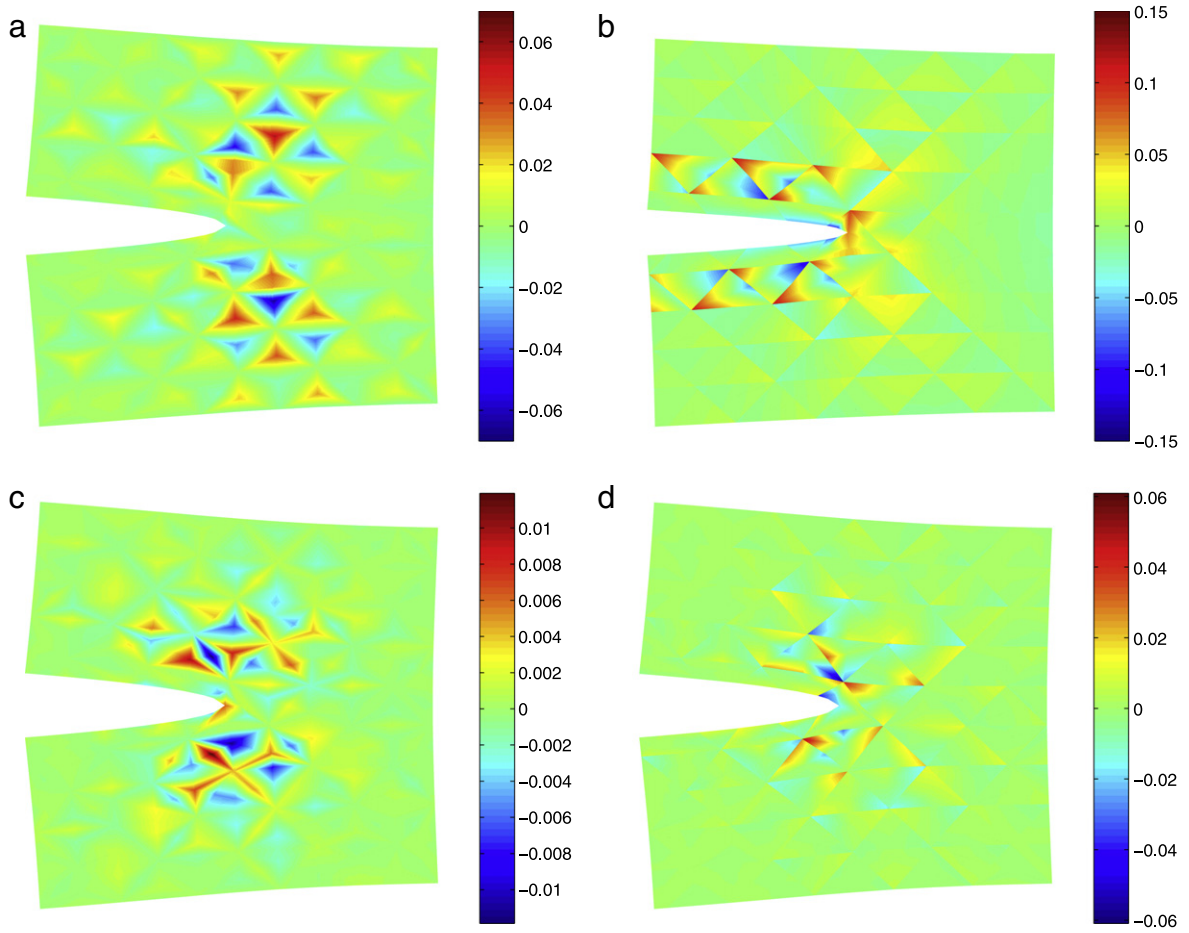


Fig. 22. Exact error for the  $y$ -component of stress. Topologic pattern of enrichment with singular functions (6) over the mesh M2 of Fig. 13. Polynomial enrichment functions (5) uniformly applied along the domain. (a)  $C^k$  approximation with  $b = 1$ . (b)  $C^0$  approximation with  $b = 1$ . (c)  $C^k$  approximation with  $b = 2$ . (d)  $C^0$  approximation with  $b = 2$ .

Table 1

Comparison between rates of convergence for  $h$ -version considering, firstly, singular enrichment according to the geometric pattern and uniformly applied polynomial enrichment and, secondly, singular enrichment according to the topologic pattern over uniform  $b = 1, 2$  discretizations and locally applied polynomial enrichment. Crack opening over element edges (Figs. 2 and 12). The degrees  $p(C^0)/p(C^k)$  refer to the degrees of polynomial enrichment applied on the seven nodes around the crack tip, in Fig. 12, for the  $C^0$  and  $C^k$  approximations, respectively. Theoretical values provided by [65].

Enrichment pattern	PoU	$b = 1$	$b = 2$	$b = 3$	$b = 4$
Geometric R1	$C^0$	0.33	0.91	1.37	1.39
	$C^\infty$	0.46	1.16	1.22	1.10
Geometric R2	$C^0$	0.24	0.73	1.06	0.90
	$C^\infty$	0.35	0.90	0.80	0.20
		$p = 0/p = 1$	$p = 1/p = 2$	$p = 2/p = 3$	$p = 3/p = 4$
Topologic ( $b = 1$ )	$C^0$	0.05	0.04	0.02	0.00
	$C^\infty$	0.13	0.13	0.14	0.14
Topologic ( $b = 2$ )	$C^0$	–	0.14	0.10	0.08
	$C^\infty$	–	0.29	0.30	0.32
Theoretical value (category A)		0.50	1.00	1.50	2.00
Theoretical value (category B)		0.25	0.25	0.25	0.25

the smooth version always shows smaller errors for a given number of DOF, whether the crack cuts elements or not. The rates of convergence for the  $C^k$ -GFEM are also higher than the rates obtained for the  $C^0$  version.

The smoothness around the crack tip avoids high stress jumps around the singularity in  $C^0$ -GFEM/XFEM approximations enriched with singular functions. In conclusion, smoothness is important in the presence of a singularity introduced via extrinsic enrichments in PoU-based methods. Such a feature is related to a smaller propagation of error beyond the singularity neighborhood. In other words, in the  $C^k$  approximations there are not errors due to the product between stress discontinuities and the singular enrichment functions over the interelement edges around the crack tip, as occur in  $C^0$  models. This fact may be better observed by assessing local measures as stress intensity factors. This investigation, considering the configurational forces method [74], has been conducted by the present authors and will be the topic of a forthcoming paper. Thus, the higher accuracy of the  $C^k$ -GFEM in the singular enrichment zone is particularly significant and important for LEFM problems.

The results suggest that  $C^k$ -GFEM-based higher regularity PoU functions offer a better representation of the singular enrichment applied for crack modeling. The flat-top property of  $C^k$ -GFEM PoU has shown to be a very good alternative for incorporating the information provided by the singular enrichment functions (6) of conventional XFEM [10] in the ansatz. The flat-top allows the reproduction of the singular enrichment with greater fidelity, and this property has been noted as a desirable feature of a PoU function [47,48]. This effect can be noted from the low dependence on the pattern of enrichment, and the conclusion is supported by the higher eigenvalues of the stiffness matrix of  $C^k$ -GFEM, compared to the standard  $C^0$  version (continuous lines in Fig. 10, for instance), and from the smaller values of error in stress in the crack tip neighborhood, Figs. 21 and 22.

Thus, with regard to conditioning, this work reveals two important features of GFEM/XFEM. The first is related to the higher incorporation of the strain energy associated with the singular enrichment functions by the smooth  $C^k$  PoU. This fact was enlightened by the eigenvalues distributions, which showed that  $C^k$ -GFEM generates higher eigenvalues than  $C^0$ -GFEM/XFEM (Fig. 10(a), for example). The second important observation is related to the polynomial enrichment, considering functions as in (5), mainly when such polynomial enrichment is uniformly applied. This type of polynomial enrichment generates very low eigenvalues that can rapidly lead to ill-conditioning, and as previously stated, it requires additional research on different types of polynomial enrichment.

A natural next step of this investigation is to evaluate the behavior of  $C^k$ -GFEM considering modified enrichments according to the stable GFEM strategy [79,80]. Of course, some improvements already noticed for  $C^0$ -GFEM/XFEM could also be verified for smooth discretizations. Stable GFEM (SGFEM) modifies the enrichments and requires a special care in choosing the appropriate nodes for enrichment (see Fig. 9, page 30, of [80]), as the method requires the evaluation of the original enrichment functions at all nodes of a finite element, to obtain its finite element interpolant inside the element. Here, such modification performed by the SGFEM strategy would make the experiments with a topological pattern using discretizations such as the ones displayed in Fig. 12 unfeasible.

Another observation concerns the cost of numerical integration. This issue has been a topic of investigation for the present authors, and in the case of regular problems was approached in [51,27,28]. Efforts to reduce integration cost are needed, whether to integrate the singular enrichment or the polynomial enriched  $C^k$ -GFEM functions. The high oscillatory partial derivatives of the infinitely smooth  $C^k$ -GFEM PoU functions, as is typical of rational functions, require a considerable number of integration points. The use of polynomial cloud edge functions can contribute to reducing the cost, as already noted in [51]. Some benefits of the use of polynomial smooth PoU were reported in [81], mainly in terms of reduced integration cost, but such type of PoU imposes geometrical restrictions on the clouds. This issue requires further investigation.

Concerning singular enrichment functions, the cost of numerical integration can be reduced by applying statically admissible enrichment functions. The application of the divergence theorem as a means of substituting domain integrations for line integrations was suggested in [82]. Nevertheless, the singular enrichment functions considered in that work, similarly to those used herein (6) after [10] (the functions most commonly used for crack modeling in two-dimensional problems), do not reproduce the exact solutions, numerically at least. This observation, also reported by [83], leads to the option of applying the exact asymptotic solution [73,58] to effectively introduce the singularity, consequently consuming fewer DOF per enriched node and allowing the integration of element contributions only on the element edges, in the case of elements with equally enriched nodes. Certain other approaches have been proposed to reduce the number of enrichment functions per node in the crack tip vicinity, such as the strategy proposed in [84], which is similar to the numerically-built enrichments of [85].

Finally, smooth PoU functions are very appropriate for improving stress approximations around the singularity introduced via extrinsic enrichment. Some deleterious effects, such as conditioning deterioration and a higher number of DOF, for a given degree of reproducibility, may be strongly reduced by applying  $C^k$  PoU functions only where they are convenient: in the neighborhood of the crack tip. In this context, the  $C^k$ -GFEM is a highly robust methodology in the sense that it makes possible to vary the smoothness along the domain simply by setting different weighting functions for the nodes, following [49], in such a way that PoU functions may be built combining smooth weighting functions and  $C^0$  FE shape functions. Additionally, no enlargement of the PoU's supports is involved, in such a fashion that this  $k$ -refinement does not impact the stiffness matrix sparsity. Some experiments considering the localized application of smooth PoU functions are being conducted and new results will be presented in the future.

## Acknowledgments

Diego A. F. Torres gratefully acknowledges the financial support provided by the Brazilian government agency CNPq (Conselho Nacional de Desenvolvimento Científico e Tecnológico) for this research, under the Ph.D. and postdoctoral scholarships, 140.713/2008-5 and 163.461/2012-0, respectively. Clovis S. de Barcellos and Paulo T. R. Mendonça also acknowledge the support provided by CNPq under research grants 303.315/2009-1 and 303.575/2010-7, respectively. The authors also thank Professor C. Armando Duarte of the Department of Civil and Environmental Engineering, University of Illinois at Urbana–Champaign, for fruitful discussions on some aspects of this work.

## References

- [1] T. Belytschko, R. Gracie, G. Ventura, A review of extended/generalized finite element methods for material modeling, *Model. Simul. Mater. Sci. Eng.* 17 (2009) 043001.
- [2] F.B. Barros, S.P.B. Proença, C.S. de Barcellos, On error estimator and  $p$ -adaptivity in the generalized finite element method, *Internat. J. Numer. Methods Engrg.* 60 (2004) 2373–2398.
- [3] F.B. Barros, C.S. de Barcellos, C.A. Duarte,  $-p$  Adaptive  $C^k$  generalized finite element method for arbitrary polygonal clouds, *Comput. Mech.* 42 (2007) 175–187.
- [4] K.S. Surana, S.R. Petti, A.R. Ahmadi, J.N. Reddy, On  $p$ -version hierarchical interpolation functions for higher-order continuity finite element models, *Int. J. Comput. Appl. Math.* 2 (2001) 653–673.
- [5] H.C. Edwards,  $C^\infty$  finite element basis functions. Technical Report, TICAM Report 96-45, The University of Texas at Austin, 1996.
- [6] J.A. Cottrell, T.J.R. Hughes, A. Reali, Studies of refinement and continuity in isogeometric structural analysis, *Comput. Methods Appl. Mech. Engrg.* 196 (2007) 4160–4183.
- [7] P. Laborde, J. Pommier, Y. Renard, M. Salaun, High-order extended finite element method for cracked domains, *Internat. J. Numer. Methods Engrg.* 64 (2005) 354–381.
- [8] E. Béchet, H. Minnebo, N. Moës, B. Burgardt, Improved implementation and robustness study of the XFEM for stress analysis around cracks, *Internat. J. Numer. Methods Engrg.* 64 (2005) 1033–1056.
- [9] C.A. Duarte, D.-J. Kim, D.M. Quaresma, Arbitrarily smooth generalized finite element approximations, *Comput. Methods Appl. Mech. Engrg.* 196 (2006) 33–56.
- [10] T. Belytschko, T. Black, Elastic crack growth in finite elements with minimal remeshing, *Internat. J. Numer. Methods Engrg.* 45 (1999) 601–620.
- [11] D. Shepard, A two-dimensional interpolation function for irregularly-spaced data. Proceedings of the 23rd ACM National Conference - ACM'68, New York, USA, 1968, 517–524.
- [12] V.L. Rvachev, Theory of  $R$ -functions and some of its applications. 1982, Naukova Dumka (in Russian).
- [13] V. Shapiro, Semi-analytic geometry with  $R$ -functions, *Acta Numer.* 16 (2007) 239–303.
- [14] P. Lancaster, K. Salkauskas, Surfaces generated by moving least squares methods, *Math. Comp.* 137 (1981) 141–158.
- [15] S. De, K.J. Bathe, The method of finite spheres, *Comput. Mech.* 25 (2000) 329–345.
- [16] M. Griebel, M.A. Schweitzer, A particle-partition of unity method for the solution of elliptic, parabolic and hyperbolic PDEs, *SIAM J. Sci. Comput.* 22 (2000) 853–890.
- [17] T. Belytschko, Y.Y. LU, L. Gu, Element-free Galerkin method, *Internat. J. Numer. Methods Engrg.* 37 (1994) 229–256.
- [18] T.-P. Fries, T. Belytschko, The intrinsic XFEM: a method for arbitrary discontinuities without additional unknowns, *Internat. J. Numer. Methods Engrg.* 68 (2006) 1358–1385.
- [19] G.R. Liu, *Mesh Free Methods: Moving Beyond the Finite Element Method*, CRC Press, Boca Raton, 2003.
- [20] C.A. Duarte, J.T. Oden,  $hp$  clouds - a meshless method to solve boundary-value problems. Technical Report, TICAM, The University of Texas at Austin, 1995.
- [21] C.A. Duarte, J.T. Oden, An  $h$ - $p$  adaptive method using cloud, *Comput. Methods Appl. Mech. Engrg.* 139 (1996) 237–262.
- [22] J.T. Oden, C.A. Duarte, O.C. Zienkiewicz, A new cloud-based  $hp$  finite element method, *Comput. Methods Appl. Mech. Engrg.* 153 (1998) 117–126.
- [23] J.M. Melenk, I. Babuška, The partition of unity finite element method: basic theory and applications. Technical Report, TICAM, The University of Texas at Austin, 1996, Report 96-01.

- [24] C.A. Duarte, I. Babuška, J.T. Oden, Generalized finite element method for three-dimensional structural mechanics problems, *Comput. Struct.* 77 (2000) 215–232.
- [25] O.A. Garcia, E.A. Fancello, P.T.R. Mendonça, Developments in the application of the generalized finite element method to thick shell problems, *Comput. Mech.* 44 (2009) 669–682.
- [26] D.A.F. Torres, P.T.R. Mendonça, C.S. de Barcellos, Evaluation and verification of an HSDT-Layerwise generalized finite element formulation for adaptive piezoelectric laminated plates, *Comput. Methods Appl. Mech. Engrg.* 200 (2011) 675–691.
- [27] P.T.R. Mendonça, C.S. de Barcellos, D.A.F. Torres, Analysis of anisotropic Mindlin plate model by continuous and non-continuous GFEM, *Finite Elem. Anal. Des.* 47 (2011) 698–717.
- [28] P.T.R. Mendonça, C.S. de Barcellos, D.A.F. Torres, Robust  $C^k/C^0$  generalized FEM approximations for higher-order conformity requirements: application to Reddy's HSDT model for anisotropic laminated plates, *Compos. Struct.* 96 (2013) 332–345.
- [29] I. Babuška, J.M. Melenk, The partition of unity finite element method, *Internat. J. Numer. Methods Engrg.* 40 (1997) 727–758.
- [30] G.R. Liu, K.Y. Dai, T.T. Nguyen, A smoothed finite element method for mechanics problems, *Comput. Mech.* 39 (2007) 859–877.
- [31] J.S. Chen, C.T. Wu, S. Yoon, Y. You, A stabilized conforming nodal integration for Galerkin meshfree method, *Internat. J. Numer. Methods Engrg.* 50 (2001) 435–466.
- [32] S. Beissel, T. Belytschko, Nodal integration of the element-free Galerkin method, *Comput. Methods Appl. Mech. Engrg.* 139 (1996) 49–74.
- [33] H.H. Zhang, S.-J. Liu, L.-X. Li, On the smoothed finite element method, *Internat. J. Numer. Methods Engrg.* 76 (2008) 1285–1295.
- [34] S.P.A. Bordas, S. Natarajan, On the approximation in the smoothed finite element method, *Internat. J. Numer. Methods Engrg.* 81 (2010) 660–670.
- [35] E.L. Wachspress, *A Rational Finite Element Basis*, Academic Press, New York, 1975.
- [36] G. Dasgupta, Interpolants with convex polygons: Wachspress's shape functions, *J. Aerosp. Eng.* 16 (2003) 1–8.
- [37] N. Sukumar, E.A. Malsch, Recent advances in the construction of polygonal finite element interpolants, *Arch. Comput. Methods Eng.* 13 (2006) 129–163.
- [38] N. Sukumar, A. Tabarraei, Conforming polygonal finite elements, *Internat. J. Numer. Methods Engrg.* 82 (2004) 2045–2066.
- [39] H. Hiyoshi, K. Sugihara, Two generalizations of an interpolant based on Voronoi diagrams, *Int. J. Shape Model.* 5 (1999) 219–231.
- [40] C. Talischi, G.H. Paulino, A. Pereira, I.F.M. Menezes, Polygonal finite elements for topology optimization: a unifying paradigm, *Internat. J. Numer. Methods Engrg.* 82 (2010) 671–698.
- [41] A. Tabarraei, N. Sukumar, Extended finite element method on polygonal and quadtree meshes, *Comput. Methods Appl. Mech. Engrg.* 197 (2008) 425–438.
- [42] M. Arroyo, M. Ortiz, Local maximum-entropy approximation schemes: a seamless bridge between finite elements and meshfree methods, *Internat. J. Numer. Methods Engrg.* 65 (2006) 2167–2202.
- [43] F. Amiri, C. Anitescu, M. Arroyo, S.P.A. Bordas, T. Rabczuk, XLME interpolants, a seamless bridge between XFEM and enriched meshless methods, *Comput. Mech.* 53 (2014) 45–57.
- [44] H.-S. Oh, J.W. Jeong, W.-T. Hong, The generalized product partition of unity for the meshless methods, *J. Comput. Phys.* 229 (2010) 1600–1620.
- [45] M.A. Schweitzer, *Meshfree and generalized finite element methods (Habilitation thesis)*, R.F.-W. Universität Bonn, 2008.
- [46] R. Tian, G. Yagawa, H. Terasaka, Linear dependence problems of partition of unity-based generalized FEMs, *Comput. Methods Appl. Mech. Engrg.* 195 (2006) 4768–4782.
- [47] H.-S. Oh, J.G. Kim, W.-T. Hong, The piecewise polynomial partition of unity functions for the generalized finite element methods, *Comput. Methods Appl. Mech. Engrg.* 197 (2008) 3702–3711.
- [48] W.-T. Hong, P.-S. Lee, Mesh based construction of flat-top partition of unity functions, *Appl. Math. Comput.* 219 (2013) 8687–8704.
- [49] C.A. Duarte, D.Q. Migliano, E.B. Baker, A technique to combine meshfree- and finite element-based partition of unity approximations. Technical Report. Department of Civil and Environmental Engineering. University of Illinois at Urbana-Champaign, 2005.
- [50] J.T. Oden, J.N. Reddy, *An Introduction to the Mathematical Theory of Finite Elements*, John Wiley and Sons, New York, 1976.
- [51] C.S. de Barcellos, P.T.R. Mendonça, C.A. Duarte, A  $C^k$  continuous generalized finite element formulations applied to laminated Kirchhoff plate model, *Comput. Mech.* 44 (2009) 377–393.
- [52] V.L. Rvachev, T.I. Sheiko,  $R$ -functions in boundary value problems in mechanics, *Appl. Mech. Rev.* 48 (1995) 151–188.
- [53] N. Moës, J. Dolbow, T. Belytschko, A finite element method for crack growth without remeshing, *Internat. J. Numer. Methods Engrg.* 46 (1999) 131–150.
- [54] I. Babuška, J.R. Whiteman, T. Strouboulis, *Finite Elements: An Introduction to the Method and Error Estimation*, Oxford, New York, 2011.
- [55] C.A. Brebbia, J.C.F. Telles, L.C. Wrobel, *Boundary Element Techniques: Theory and Applications in Engineering*, Springer-Verlag, Berlin, 1984.
- [56] D. Schillinger, J.A. Evans, A. Reali, M.A. Scott, T.J.R. Hughes, Isogeometric collocation: cost comparison with Galerkin methods and extension to adaptive hierarchical NURBS discretizations, *Comput. Methods Appl. Mech. Engrg.* 267 (2013) 170–232.
- [57] R. Schaback, H. Wendland, Kernel techniques: from machine learning to meshless methods, *Acta Numer.* 15 (2006) 543–639.
- [58] T.L. Anderson, *Fracture Mechanics: Fundamentals and Applications*, third ed., CRC Press, Boca Raton, 2005.
- [59] T. Belytschko, N. Moës, S. Usui, C. Parimi, Arbitrary discontinuities in finite elements, *Internat. J. Numer. Methods Engrg.* 50 (2001) 993–1013.
- [60] B.A. Szabó, Estimation and control of error based on  $p$ -convergence, in: I. Babuška (Ed.), *Accuracy Estimates and Adaptive Refinements in Finite Element Computations*, Wiley Series in Numerical methods in Engineering, 1986, pp. 61–78.
- [61] J. Chessa, H. Wang, T. Belytschko, On the construction of blending elements for local partition of unity enriched finite elements, *Internat. J. Numer. Methods Engrg.* 57 (2003) 1015–1038.
- [62] J.E. Taracón, A. Vercher, E. Giner, F.J. Fuenmayor, Enhanced blending elements for XFEM applied to linear elastic fracture mechanics, *Internat. J. Numer. Methods Engrg.* 77 (2009) 126–148.

- [63] F.L. Stazi, E. Budyn, J. Chessa, T. Belytschko, An extended finite element method with higher-order elements for curved cracks, *Comput. Mech.* 31 (2003) 38–48.
- [64] B. Szabó, A. Duster, E. Rank, The  $p$ -version of the finite element method, in: E. Stein, R. de Borst, T.J.R. Hughes (Eds.), *Encyclopedia of Computational Mechanics*, Wiley, 2004.
- [65] B. Szabó, I. Babuška, *Introduction to Finite Element Analysis: Formulation, Verification and Validation*, Wiley, Chichester, United Kingdom, 2011.
- [66] K. Park, J.P. Pereira, C.A. Duarte, G.H. Paulino, Integration of singular enrichment functions in the generalized/extended finite element method for three-dimensional problems, *Internat. J. Numer. Methods Engrg.* 78 (2009) 1220–1257.
- [67] Q. Xiao, B. Karihaloo, Improving the accuracy of XFEM crack tip fields using higher order quadrature and statically admissible stress recovery, *Internat. J. Numer. Methods Engrg.* 66 (2006) 1378–1410.
- [68] S. Natarajan, D.R. Mahapatra, S.P.A. Bordas, Integrating strong and weak discontinuities without integration subcells and example applications in an XFEM/GFEM framework, *Internat. J. Numer. Methods Engrg.* 83 (2010) 269–294.
- [69] D. Xu, H. Zheng, K. Xia, New numerical quadrature of integrand with singularity of  $1/r$  and its application, *Appl. Mech. Mater.* 444–445 (2014) 641–649.
- [70] J.C. Lachat, J.O. Watson, Effective numerical treatment of boundary integral equations: a formulation for three dimensional elastostatic, *Internat. J. Numer. Methods Engrg.* 10 (1976) 991–1005.
- [71] R.S. Barsoum, Application of quadratic isoparametric element in linear fracture mechanics, *Int. J. Fract.* 10 (1974) 603–605.
- [72] S. Wandzura, H. Xiao, Symmetric quadrature rules on a triangle, *Comput. Math. Appl.* 45 (2003) 1829–1840.
- [73] M. Williams, On the stress distribution at the base of a stationary crack, *ASME J. Appl. Mech.* 24 (1957) 109–114.
- [74] P. Steinmann, M. Scherer, R. Denzer, Secret and joy of configurational mechanics: from foundations in continuum mechanics to applications in computational mechanics, *J. Appl. Math. Mech.* 89 (2009) 614–630.
- [75] D. Cho, A note on the singular linear system of the generalized finite element methods, *Appl. Math. Comput.* 217 (2011) 6691–6699.
- [76] B. Szabó, I. Babuška, *Finite Element Analysis*, John Wiley and Sons, New York, 1991.
- [77] E. Chahine, P. Laborde, Y. Renard, A quasi-optimal convergence result for fracture mechanics with XFEM, *C. R. Math.* 342 (2006) 527–532.
- [78] A. Freitas, D.A.F. Torres, P.T.R. Mendonça, C.S. de Barcellos, Comparative analysis of  $C^k$ - and  $C^0$ -GFEM applied to two-dimensional problems of confined plasticity, *Lat. Am. J. Solids Struct.* (2014) in press.
- [79] I. Babuška, U. Banerjee, Stable generalized finite element method (SGFEM), *Comput. Methods Appl. Mech. Engrg.* 201–204 (2012) 91–111.
- [80] V. Gupta, C.A. Duarte, I. Babuška, U. Banerjee, A stable and optimally convergent generalized FEM (SGFEM) for linear elastic fracture mechanics, *Comput. Methods Appl. Mech. Engrg.* 266 (2013) 23–39.
- [81] M. Kumar, S. Chakravorth, P. Singla, J.L. Junkins, The partition of unity finite element approach with  $hp$ -refinement for the stationary Fokker–Planck equation, *J. Sound Vib.* 327 (2009) 144–162.
- [82] G. Ventura, R. Gracie, T. Belytschko, Fast integration and weight function blendign in the extended finite element method, *Internat. J. Numer. Methods Engrg.* 77 (2009) 1–29.
- [83] T. Gerasimov, M. Ruter, E. Stein, An explicit residual-type error estimator for  $Q_1$ -quadrilateral extended finite element method in two-dimensional linear elastic fracture mechanics, *Internat. J. Numer. Methods Engrg.* 90 (2012) 1118–1155.
- [84] S. Natarajan, C. Song, Representation of singular fields without asymptotic enrichment in the extended finite element method, *Internat. J. Numer. Methods Engrg.* 96 (2013) 813–841.
- [85] D.-J. Kim, J.P. Pereira, C.A. Duarte, Analysis of three-dimensional fracture mechanics problems: a two-scale approach using coarse generalized FEM meshes, *Internat. J. Numer. Methods Engrg.* 81 (2010) 335–365.